FACTORS CONTRIBUTING TO RIGIDITY EXPRESSION AND RESPONSE TO PALLIDAL DEEP BRAIN STIMULATION IN PEOPLE WITH PARKINSON'S DISEASE

A DISSERTATION SUBMITTED TO THE FACULTY OF

THE UNIVERSITY OF MINNESOTA BY

Maria Elizabeth Linn-Evans

IN PARTIAL FULFILLMENT OF THE REQUIREMENTS

FOR THE DEGREE OF DOCTOR OF PHILOSOPHY

Advised by Colum D. MacKinnon, PhD

September 2021

ACKNOWLEDGEMENTS

I'd like to start by thanking the University of Minnesota Graduate Program in Neuroscience and the numerous funding sources that have supported my training: NIH 4T32GM008471-24 Predoctoral Training of Neuroscientists Training Grant, NSF DGE-1734815 NRT Graduate Training Program in Sensory Science Fellowship, NIH R01 NS088679 "Predictors of progression to freezing of gait in Parkinson's disease", and NIH P50 NS098573 "Circuit-based deep brain stimulation for Parkinson's disease".

Thank you to the members of my thesis committee, Drs. Jürgen Konczak, Matthew Johnson, and Bernadette Gillick for all the guidance and encouragement they have provided throughout my PhD training. I am especially thankful for all of their kindness and understanding during difficult times, and always working to help me find a way to move forward with my research. I'd especially like to thank Matt Johnson for his endless patience while spending so much time in the last year teaching me about computational modeling.

I'd also like to thank my incredible advisor and lab - it takes a village to raise a PhD student, and I am so unbelievably thankful that the Movement Disorders Lab raised me. I could not have asked for a better advisor throughout these past few years than Dr. Colum MacKinnon – he has advised me with kindness, patience, and thoughtfulness while always taking the time to remind me that it is okay to be human. Not only has he told me this in words, but also through his actions, including taking up new hobbies like bagpiping and making sure to spending quality time with his family. In addition to my formal advising team, I have also been blessed to have Sommer Amundsen Huffmaster as my mentor extraordinaire. Sommer has provided so much guidance in academia and in life, and I've loved getting to go through so many milestones together (weddings and babies and PhDs, oh my!) I am so proud of her accomplishments as a woman in science and engineering and I gained so much confidence in myself by following her example. I'd also like to thank the other MDL members that have been so welcoming and encouraging: Josh DeKam, for helping will all things recruitment related, Dr. Rebekah Summers, for being the best desk neighbor and lab big sister, Dr. Jae Woo Chung, for

sharing so much knowledge and always being patient with me, and Dr. Matt Petrucci, for helping me start my reign as Rigidity Queen.

Thank you to the caring staff at Boynton Health and the M Health Clinics and Surgery Center, especially Christina Eichstadt, Christina Walker, and Dr. Maria Evasovich. I never expected that one of my PhD challenges would be a thyroid cancer diagnosis, and I am so grateful that I had such a kind team of health professionals to help me manage my mental and physical health during this time.

I also need to send an enormous shoutout the amazing friends that I've made in graduate school – there are no words for the amount of gratitude I have for them. I never anticipated that I would become so close to my entire graduate school cohort, but now I can't imagine my life without them. To the 2016 GPN Cohort: Jenn Brown, Natalie Lopresti, Carey Lyons, Megan Monko, Tim Monko, Carlee Toddes, and Roman Tyshynsky – thank you for W(h)ine Wednesdays, Friday Happies, endless pet photos, and providing unwavering support to each other through all the hurdles these past five years have thrown our way.

One of the best decisions I've made was to choose a graduate program close to my family. Thank you to my family for encouraging me and loving me during this PhD process, even when I made it hard. I'm especially grateful for Jason Linn, my younger brother and PhD pal, who never fails to show up with the right bottle of wine and good story when I'm having a bad day. And of course, I can never give enough thanks for my amazing parents, Jenny and Bruce Linn, who never hesitated to support my scientific endeavors, whether it was buying me science books and driving me to science fairs in elementary school or listening to all my excitement as I talked about my graduate research. Thank you for never letting me doubt for a minute that I belonged in science. And thank you for feeding me so many meals from your fridge and letting me use your giant bathtub when I needed a break from being a responsible adult. I couldn't have done any of this without you, and I hope I've made you proud.

And finally, to Isaac Evans, my incredible partner and husband. When we met at age 16, I'm sure you never imagined I'd want to be a student for the next 11 years. Thank you for listening to my neuroscience rants, cooking dinner for me when I had I long day

in lab, and telling me that you love when I get excited about my research. You are the best partner I could have asked for, thank you for loving me through all of this and more.

DEDICATION

This dissertation is dedicated to the brave women who persevered in their scientific endeavors despite the monumental barriers they faced. They paved the way for all of us, and I hope to honor their legacy by embodying the message that **science is for everyone**.

"Science and everyday life cannot and should not be separated" – Rosalind Franklin

ABSTRACT

Parkinson's disease (PD) is a neurodegenerative disorder characterized by the loss of dopaminergic cells in the substantia nigra, buildup of alpha-synuclein in specific regions of the brain, and the emergence of cardinal motor symptoms including rigidity, slowness of movement, tremor, and gait dysfunction. Despite these shared characteristics, there is a great deal of heterogeneity in symptom presentation and response to therapies within the population of individuals with PD. Understanding the driving factors behind this heterogeneity is crucial for developing targeted and effective therapies for the disease and improving outcomes for those living with Parkinson's disease. In this dissertation, two studies are described: 1) an investigation into the effects of rapid eye movement (REM) sleep without atonia (RSWA) on the presentation of rigidity in a population of individuals with mild-to-moderate Parkinson's disease and 2) the development and implementation of a computational model of pallidal deep brain stimulation (GP-DBS) to identify neural pathways associated with rigidity suppression in individuals with PD. Both studies utilize a quantitative measure of rigidity as a tool to assess symptom severity. In the first study, our findings demonstrate that people with mild to moderate PD and RSWA have dysfunctional regulation of muscle tone during both sleep and wakefulness. The results show that the presence of RSWA is associated with increased forearm rigidity magnitude and symmetry. In the second study, a patient-specific computational model of GP-DBS was developed and implemented. By combining pathway activation estimates from the model with quantitative measurements of rigidity, the analyses identified the internal capsule as an important pathway for reducing parkinsonian rigidity. In particular, profound decreases in rigidity were associated with activation of internal capsule fibers projecting from Brodmann's area 6, which contains axons from premotor cortex and supplementary motor area. The results of these studies reveal the importance of understanding factors like RSWA that may drive heterogeneity in PD, while also identifying potential pipelines for developing symptom-specific targets for treatment.

TABLE OF CONTENTS

LIST OF TABLES

LIST OF FIGURES

LIST OF ABBREVIATIONS

BA6 Brodmann's area 6

CT Computed tomography

DBS Deep brain stimulation

DWI Diffusion weighted imaging

FEM Finite element model

GABA γ-aminobutyric acid

GP Globus pallidus

GP-DBS Globus pallidus deep brain stimulation

GPi Globus pallidus internus

GPe Globus pallidus externus

IC Internal capsule

LDE Levodopa daily equivalent

LME Linear mixed-effect

M1 Primary motor cortex

mA Milliamperes

MDS-UPDRS Movement Disorder Society Unified Parkinson's Disease Rating Scale

MRI Magnetic resonance imaging

PD Parkinson's disease

RBD Rapid eye movement sleep behavior disorder

REM Rapid eye movement

RSWA Rapid eye movement sleep without atonia

SMA Supplementary motor area

SN Substantia nigra

STN Subthalamic nucleus

V Volts

VTA Volume of tissue activated

CHAPTER 1 INTRODUCTION

1.1 Parkinson's Disease

Parkinson's disease (PD) is the 2nd most prevalent neurodegenerative disease affecting nearly one million people in the United States, with numbers expected to grow significantly over the next decade as the population ages (Marras et al., 2018). PD is characterized by the loss of dopaminergic neurons in the substantia nigra pars compacta as well as the presence of abnormal alpha-synuclein protein aggregates known as Lewy bodies in specific regions of the brain. This loss of dopaminergic input causes dysfunction in the basal ganglia, leading to the emergence of the cardinal motor symptoms of PD which are tremor, slowness of movement, rigidity, and gait and postural disturbances (Kalia & Lang, 2015). While dopamine replacement therapy can effectively treat most PD motor symptoms early in the disease, in later stages the use of dopaminergic drugs can lead to uncomfortable side effects such as dyskinesias and provides inconsistent symptom management. There are currently no disease-modifying treatment options for PD, making the goal of treatment to reduce symptoms and improve quality of life. The National Institute of Neurological Disorders and Stroke suggests that research into PD focuses on specific goals, two of which are addressed in this dissertation: understanding the mechanisms that underlie its heterogeneity in clinical presentation, and optimizing current treatment options for individuals living with PD (Knopman, 2014). With the prevalence of PD expected to increase drastically in the next decade, it is becoming more important than ever to pursue these research recommendations in order to improve the quality of life of our aging population and reduce the economic burden of the disease (Kowal, Dall, Chakrabarti, Storm, & Jain, 2013). The work presented in this dissertation uses rigidity, a cardinal motor symptom of PD, as a lens through which the issues of heterogeneity of symptom presentation in PD and deep brain stimulation efficacy are explored.

1.2 Physiology of Rigidity

Rigidity is a cardinal motor symptom of PD defined as resistance of a body segment to imposed passive movement due to excessive muscle tone. It can present in the joints of the upper and lower limbs as well as in the neck and trunk, and is often described as a

tightness or stiffness by people with PD. Rigidity is a common symptom within the population of individuals with PD and can often be detected early in the disease (Martin, Loewenson, Resch, & Baker, 1973; Mutch, Strudwick, Roy, & Downie, 1986; R. B. Postuma, Lang, Gagnon, Pelletier, & Montplaisir, 2012). In addition to its prevalence, rigidity is also significantly correlated with the progression of disease as defined by the loss of dopaminergic cells within the substantia nigra, making it a useful non-invasive marker of disease progression (Francois, Vingerhoets, Schulzer, Calne, & Snow, 1997). Rigidity responds well to both dopaminergic drugs and deep brain stimulation and thus serves as a valuable symptom for assessing the efficacy of treatments (Paul Krack, Fraix, Mendes, Benabid, & Pollak, 2002; Yahr, Duvoisin, Schear, Barrett, & Hoehn, 1969).

Alterations in both spinal and supraspinal processing of proprioceptive sensory input have been implicated in the pathogenesis of rigidity in PD. The magnitude of the long-latency stretch reflex (thought to be driven by a transcortical reflex pathway via the primary motor cortex (Angel & Lemon, 1975; Colum D. MacKinnon, Verrier, & Tatton, 2000)) has been shown to be abnormally elevated in people with PD, particularly in those with the akinetic-rigid phenotype of disease (Berardelli, Sabra, & Hallett, 1983; Mortimer & Webster, 1979; Tatton & Lee, 1975). This finding suggests that increased excitability of sensorimotor cortex may result in abnormally enhanced muscle contractions in response to stretch, thus contributing to rigidity. This change in sensorimotor cortex excitability likely stems from alterations in basal ganglia-thalamocortical pathways due to the loss of dopaminergic innervation of the striatum, since levodopa reduces long-latency reflexes and suppresses rigidity (M. T. V. Johnson et al., 1994; Yahr et al., 1969).

Changes in spinal interneuron activity have also been suggested as a mechanism mediating rigidity (Delwaide, 2001). Dysfunction of spinal pathways mediating group Ia reciprocal inhibition and group Ib autogenetic inhibition have been proposed to contribute to increased muscle tone and stretch-evoked muscle activity in PD (Delwaide, Pepin, & Maertens De Noordhout, 1991). In particular, changes in Ib interneuron activity have been implicated in the shortening reaction, an abnormal contractile response evoked in a shortened muscle while an antagonist muscle is stretched, thus producing co-contraction and resistance to passively induced joint motion (Ruiping Xia, Sun, & Threlkeld, 2009). These abnormalities seen in spinal interneuron activity may reflect

alterations in the function of descending spinal pathways, such as the reticulospinal tract, which provides modulatory input to spinal premotor neurons (e.g. Ia and Ib interneurons), and who's output nuclei can degenerate in people with PD (Braak et al., 2003).

1.3 Measuring Rigidity

In clinical settings, rigidity is evaluated using the Movement Disorder Society Unified Parkinson's Disease Rating Scale (MDS-UPDRS), which ranges from 0-4 with specific descriptions for each score (Goetz et al., 2008). Clinicians are instructed to judge rigidity "on slow passive movement of major joints with the patient in a relaxed position and the examiner manipulating the limbs and neck." A score of 0 indicates "no rigidity" while a 4 is given for "rigidity detected without the activation maneuver and full range of motion not achieved." The activation maneuver refers to performing voluntary movements with the untested limb, such as finger tapping, which is a technique used to elicit or enhance rigidity in PD. In fact, a score of 1 on the MDS-UPDRS is defined as "rigidity only detected with the activation maneuver," which is commonly seen in people with mild PD. Throughout this dissertation, rigidity testing will be performed with and without an activation maneuver in order to capture accurate rigidity scores in individuals who may have a mild symptom presentation.

While the MDS-UPDRS is well-established in clinical settings, numerous research groups have developed quantitative methods for measuring rigidity in PD. These methods include devices implementing servomotors to move limbs at a consistent velocity, inertial measuring units to measure acceleration, and electromyography to measure muscle activity during rigidity testing (Ferreira-sánchez, Moreno-verdú, & Cano-de-la-cuerda, 2020). The quantitative rigidity scores presented in this dissertation were collected with a servomotor-driven device that simultaneously moves the forearm through pronation-supination while measuring the torque applied to the handle of the device. The device has been tested for both reliability and validity. Reliability was evaluated from rigidity scores collected from 5 healthy adults at 3 timepoints, each separated by one week. The test-retest reliability coefficient was 0.95 with a $p < 0.001$, indicating excellent reliability. Validity was evaluated by calculating the correlation between quantitative rigidity scores collected from 42 individuals with mild to moderate

PD and the MDS-UPDRS upper extremity rigidity scores from the same individuals. There was a significant correlation ($p < 0.001$, Spearman's rho = 0.48) between the manipulandum-measured rigidity scores and the MDS-UPDRS scores suggesting that this tool is a valid measurement of parkinsonian rigidity.

1.4 REM Sleep Behavior Disorder and Parkinson's Disease

Despite being defined by a set of cardinal motor symptoms, Parkinson's disease presentation varies greatly between individuals. People with PD exhibit heterogeneity in a variety of domains, including their age at diagnosis, dominant symptoms, response to treatment, and rate of progression (Lewis et al., 2005). Understanding the driving factors behind this variability is crucial for developing targeted and effective therapies for the disease and has implications for clinical care (Greenland, Williams-Gray, & Barker, 2019). For example, there is evidence that tremor-dominant PD has a slower rate of progression compared to phenotypes with rigidity, akinesia, and disordered gait as the dominant symptoms (Foltynie, Brayne, & Barker, 2002). Another symptom that has been associated with differences in disease phenotype and rate of progression is a sleep disorder known as rapid eye movement (REM) sleep behavior disorder (RBD). RBD is an alpha-synucleinopathy characterized by REM sleep without atonia (RSWA), or elevated phasic and tonic muscle activity during REM sleep cycles, and dream enactment. RBD is a strong predictor that an individual will develop overt neurodegenerative disease – over 80% of people with RBD are later diagnosed with Parkinson's disease, multiple system atrophy, or dementia with Lewy bodies (Schenck, Boeve, & Mahowald, 2013). RBD is a rare condition in the general population, affecting less than 1% of the population, but around 20-50% of people with PD have comorbid RBD upon diagnosis (Jia Zhang, Xu, & Liu, 2017). In addition to those diagnosed with RBD, there is also a substantial proportion (approximately 40%) of people with PD and RSWA who do not meet the full criteria for an RBD diagnosis (Chahine, Kauta, Daley, Cantor, & Dahodwala, 2014). PD with comorbid RBD has been associated with the akinetic-rigid phenotype of PD as well a greater severity and symmetry of motor and non-motor symptoms (Kumru, Santamaria, Tolosa, & Iranzo, 2007). Even in individuals with PD without a diagnosis of RBD, the presence of RSWA may predict differences in symptom presentation that are valuable for clinical care and treatment decisions. In this

dissertation, the relationship between RSWA and parkinsonian rigidity is explored in an effort to understand how RSWA relates to the presentation of motor symptoms in PD.

1.5 Mechanisms of Deep Brain Stimulation for Parkinson's Disease

Deep brain stimulation (DBS) is a surgical treatment option for people with PD that involves applying high-frequency stimulation to neural structures via implanted electrodes with the goal of modulating abnormal activity in circuits that contribute to the expression of symptoms. The most common targets for DBS to treat PD are the subthalamic nucleus (STN) and globus pallidus (GP), two nuclei within the basal ganglia. Stimulation in both of these regions has been shown to improve symptom severity and quality of life in a number of studies (Williams, Foote, & Okun, 2014).

Prior to DBS, a common surgical practice to treat PD was pallidotomy, which involved lesioning of the motor region of globus pallidus. Due to the similarities in symptom improvement between pallidotomies and DBS, it was initially hypothesized that the electrical stimulation acted similarly to a lesion, reducing the firing rate of neurons in the targeted structure (Agnesi, Johnson, & Vitek, 2013). The mechanisms by which DBS could lead to reduced neural activity were unclear, but numerous possibilities were suggested including depolarization block of neurons (via inactivation of sodium channels or increased potassium current) and presynaptic depression of excitatory axons (M. D. Johnson, Miocinovic, McIntyre, & Vitek, 2008). While it is true that DBS does modulate somatic activity near the active electrode, more recent evidence suggests that DBS does not act like a lesion, and instead drives the output of the stimulated nucleus and modulates irregular firing patterns by directly activating axons within the stimulated nuclei (Hashimoto, Elder, Okun, Patrick, & Vitek, 2003; McIntyre, Grill, Sherman, & Thakor, 2004). Another important development in the understanding of DBS mechanisms is that in addition to stimulating axons within the target nucleus, DBS also activates fibers of passage and nearby axonal pathways which are prevalent throughout the basal ganglia (Mathai, Wichmann, & Smith, 2013). This understanding aligns well with the more recent hypothesis of movement disorders that focuses on pathological neural activity patterns, not simply the rate of firing (Agnesi et al., 2013). High frequency stimulation activates axons that become time-locked to the stimulus, which reduces

disordered patterns in the basal ganglia and leads to increased responsiveness of the thalamus to synaptic inputs. While there are still questions remaining about the ways in which DBS improves symptoms of PD, the work presented in this dissertation makes the assumption that DBS results in the activation of axons within and near the targeted nucleus.

1.6 Modeling Deep Brain Stimulation

Deep brain stimulation is an effective therapy option for many individuals with Parkinson's disease, but unfortunately, not all patients experience meaningful improvements in their symptoms (Weaver, Follett, Hur, Ippolito, & Stern, 2005). Variability in DBS responses can result from a number of factors, such as the location of the lead within the target nucleus, how the device is programmed, patient-specific neuroanatomical features, and disease phenotype. Traditional surgical methods rely on magnetic resonance imaging (MRI) to identify important anatomical features and determine the ideal stereotactic coordinates for electrode placement (Starr, Vitek, DeLong, & Bakay, 1999). While this method can result in successful DBS outcomes, selecting a set of target coordinates based on the borders of basal ganglia nuclei does not take into account important details such as the location of specific neural pathways or the behavior of stimulation based on the electrical properties of the brain. In order to improve DBS outcomes, research groups have worked to develop tools that can be used to model patient-specific anatomy in three dimensions and determine how various electrode placements and programming settings impact the spread of current in the brain (Horn et al., 2019; A. Noecker et al., 2020). These modeling tools can provide metrics such as the volume of tissue activated (VTA) or the percentage of axons activated by DBS to better predict how a patient may respond to specific settings. These computational modeling tools have been used in numerous publications and major DBS companies, including Medtronic and Boston Scientific, have begun offering DBS modeling software as a tool for clinicians in the hope that their use will improve DBS targeting and programming for patients.

1.7 Objectives and Research Goals

This dissertation addresses questions of heterogeneity in both the presentation of PD symptoms and response to deep brain stimulation through explorations of rigidity. Chapter 2 describes an investigation into the effects of REM sleep without atonia on the presentation of rigidity in a population of individuals with mild-to-moderate PD. Chapter 3 describes the development of a patient-specific model of pallidal DBS and investigates the differences in pathway activation between dorsal and ventral stimulation locations. Finally, the same pallidal DBS model is used in Chapter 4 to determine which neural pathways are associated with rigidity suppression in individuals with Parkinson's disease.

CHAPTER 2 REM SLEEP WITHOUT ATONIA (RSWA) IS ASSOCIATED WITH INCREASED RIGIDITY IN PEOPLE WITH MILD TO MODERATE PARKINSON'S DISEASE

(Reprinted with permission by Elsevier)

Linn-Evans ME*, Petrucci MN*, Amundsen Huffmaster SL, Chung JW, Tuite PJ, Howell MJ, Videnovic A, MacKinnon CD. REM sleep without atonia is associated with increased rigidity in patients with mild to moderate Parkinson's disease. Clinical Neurophysiology 2020;131:2008–16. [*co-first authors]

2.1 Introduction

Rigidity is one of the cardinal motor signs of Parkinson's disease (PD) and is characterized by a marked increase in muscle activity in response to imposed muscle stretch. Increasing rigidity correlates with greater disease severity, yet, there is considerable heterogeneity in the expression of rigidity both within and across individuals with PD, even in individuals who are considered to have an akinetic-rigid predominant phenotype of PD (Vu, Nutt, & Holford, 2012). Heterogeneity in rigidity is particularly evident in the early stages of disease. The mechanisms contributing to the expression of rigidity are poorly understood, but alterations in the excitability of both cortical and subcortical pathways mediating long-latency stretch reflexes (Rothwell, Obeso, Traub, & Marsden, 1983; Tatton & Lee, 1975) and stretch induced co-activation of agonist-antagonist muscles (R Xia, Markopoulou, Puumala, & Rymer, 2006; Ruiping

Xia, 2011; Ruiping Xia & Rymer, 2004; Ruiping Xia et al., 2009) are considered to contribute to increased resistance during imposed movements.

Muscle activity is also abnormally elevated during rapid eye movement (REM) sleep in a substantial percentage (approximately 40%) of people with PD (Chahine et al., 2014). Increased phasic or tonic muscle activity during REM sleep is termed REM sleep without atonia (RSWA) and, in conjunction with the phenomenon of dream enactment, characterizes the parasomnia of idiopathic REM sleep behavior disorder (iRBD). Idiopathic RBD affects approximately 1% of the general population, and its prevalence is near 5% in the elderly (Bradley F. Boeve et al., 2013; Haba-Rubio et al., 2018). It is now well recognized that the presence of iRBD is highly predictive of progression to a neurodegenerative disease with alpha-synuclein pathology. It has been estimated that more than 75% of people with iRBD will develop PD, multiple system atrophy, or dementia with Lewy bodies over the course of 12 years (Ronald B. Postuma et al., 2019; Schenck et al., 2013). In a cohort of patients with de novo PD, 51% exhibited movement events during REM sleep (Mollenhauer et al., 2013). It is estimated that over 40% of individuals with PD have RSWA and more than 20% have a diagnosis of iRBD (Chahine et al., 2014; Jia Zhang et al., 2017). Individuals with PD and iRBD are more likely to present with a non-tremor dominant subtype of PD (Folle, Paul, Bronstein, Keener, & Ritz, 2019; Kumru et al., 2007; R. B. Postuma, Gagnon, Vendette, Charland, & Montplaisir, 2008; Romenets et al., 2012), and are more likely to develop postural instability, gait problems including freezing of gait, and orthostatic symptoms compared to individuals with PD alone (R. B. Postuma et al., 2008; Romenets et al., 2012). Higher levels of phasic muscle activity during REM sleep is associated with increased severity and more symmetric expression of disease (Bliwise, Trotti, Greer, Juncos, & Rye, 2010). These findings suggest that among people with PD, RSWA is associated with increased pathology of both nigrostriatal and non-dopaminergic pathways.

The increased prevalence of the akinetic-rigid phenotype in people with PD and idiopathic RBD suggests that mechanisms mediating abnormally increased phasic and tonic muscle activity during REM sleep may also contribute to alterations in muscle activity regulation during wakefulness, and thus the expression of rigidity. Increased brainstem pathology in conjunction with a higher rate of disease progression may also

lead to a more symmetric presentation of rigidity in people with elevated REM sleep muscle tone. Degeneration in brainstem regions with bilateral descending projections that impact muscle tone, such as the locus coeruleus, caudal raphe, and medullary magnocellular region of the reticular formation (Braak et al., 2006), would be expected to contribute to a more symmetrical presentation of rigidity. PD symptoms also tend to become more symmetric with disease progression, reflecting increasingly bilateral degeneration of nigrostriatal dopaminergic pathways, so more rapid disease progression may lead to earlier presentation of symmetric rigidity (Marinus & van Hilten, 2015). To date, no study has used quantitative measures to compare rigidity between people with PD with and without RSWA. The purpose of this study was to examine the level and symmetry of forearm rigidity during pronation-supination using quantitative metrics in a cohort of individuals with mild to moderate PD. We hypothesized that people with PD and RSWA would present with more severe and symmetric rigidity compared with individuals with PD without RSWA and age-matched controls.

2.2 Methods

2.2.1 Participants

Forty-one people with PD (26 males, 15 females, age = 64 ± 7.5) and 20 healthy controls (8 males, 12 females, age = 60.2 ± 7.4) were included in this study (demographic summary in Table 1). Clinical diagnosis of PD was determined by movement disorders neurologists according to the Movement Disorder Society Clinical Diagnostic Criteria for PD (Ronald B. Postuma et al., 2015). Individuals in this study were part of a long-term prospective study, and those who were subsequently diagnosed with another form of parkinsonism were removed from this dataset. Exclusion criteria included: dementia diagnosis and/or a Montreal Cognitive Assessment score below 22 to screen for capacity to consent (Karlawish et al., 2013), history of a musculoskeletal disorder that significantly affects upper limb movement, other significant neurological disorders, implanted deep brain stimulator or other neurosurgery to treat PD, and insufficiently treated sleep apnea. All participants with PD performed movement tasks after a 24-hour withdrawal period from extended release antiparkinson medications and a 12-hour withdrawal period from immediate release antiparkinson medications. All study

procedures were approved by the University of Minnesota Institutional Review Board and all participants provided written informed consent according to the Declaration of Helsinki.

2.2.2 Group Assignment

All participants underwent an overnight polysomnography (PSG) study at the Sleep Center at the University of Minnesota, Fairview. Participants with PD were allowed to take antiparkinson medications for this portion of the study. The sleep studies were performed using standard video-based PSG procedures, including electromyography (EMG) recordings from the chin, forearms, and legs as well as electroencephalography recordings from 10 scalp electrodes. PSG data was analyzed by a blinded rater who is board certified in sleep medicine (A.V.). Sleep stages and percentage of REM sleep with RSWA were scored according to the American Academy of Sleep Medicine Manual for the Scoring of Sleep (Berry, Brooks, Gamaldo, Harding, & Lloyd, 2018). Participants with PD were stratified into low and high RSWA groups based on the percentage of time during REM sleep when RSWA was present. The thresholds to be considered RSWA positive were derived from the distributions of the RSWA PSG scores across subjects. Participants with RSWA in at least 1 muscle group and/or clear evidence of dream enactment were assigned to the PD-RSWA+ group. There was a significant effect of group for both the tonic and phasic chin RSWA levels ($F(2,58) = 15.4$ (tonic), 22.6 (phasic), $p < 0.001$) as well as for phasic arm RSWA levels ($F(2,51) = 15.1$, $p < 0.001$) driven by significantly higher RSWA levels in the PD-RSWA+ group compared with the PD-RSWA- group and controls ($p < 0.001$) (Figure 1). All Control participants had normal levels of EMG activity below the determined cutoffs.

Table 1. Demographics of study participants. Age was compared with a one-way ANOVA. Disease duration and levodopa daily equivalent were compared using t-tests and Bonferroni corrected for multiple comparisons. There was a significant difference in levodopa daily equivalent between the Parkinson's disease with RSWA (PD-RSWA+) and Parkinson's disease without RSWA (PD-RSWA-) groups (* $p = 0.009$). Movement Disorder Society Unified Parkinson's Disease Rating Scale part III (MDS-UPDRS III) total scores and rigidity subscores were compared between groups using independent samples Kruskal-Wallis tests. These scores were significantly higher in both Parkinson's disease groups compared to the control group (* $p < 0.001$).

	Control (n=20)	PD-RSWA- (n=19)	PD-RSWA+ (n=22)
Male/Female	8/12	13/6	13/9
Age (years)	60.2 ± 7.4	62.6 ± 8.6	65.1 ± 6.4
Disease duration (years)	N/A	2.1 ± 1.5	2.8 ± 2.2
MDS-UPDRS III Total Score (OFF medications) *	3.5 ± 2.5	35.5 ± 11.9	40.1 ± 13.8
MDS-UPDRS III Section 3.3 Rigidity Subscore *	1.0 ± 1.2	6.1 ± 3.0	7.3 ± 3.6
Levodopa daily equivalent (mg) *	N/A	225 ± 168	505 ± 416

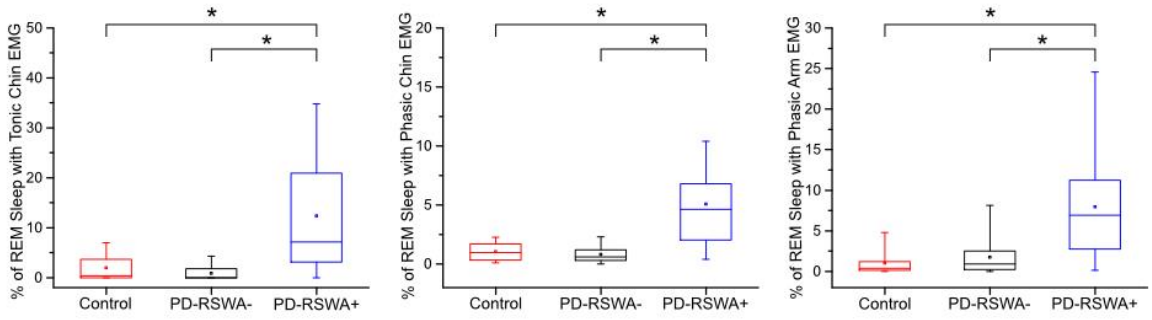

Figure 1. Rapid eye movement (REM) sleep without atonia (RSWA) values across groups. Participants were grouped by the percentage of REM sleep in which they exhibited RSWA for each of the measured muscles (submentalis or flexor digitorum superficialis). Participants who exhibited RSWA in at least one muscle group were categorized as Parkinson's disease with RSWA (PD-RSWA+) while those with no RSWA were categorized as Parkinson's disease without RSWA (PD-RSWA-). There was a significantly higher level of RSWA in the PD-RSWA+ group compared to the PD-RSWA- and control groups (One-way ANOVA, Bonferroni corrected post hoc comparisons, * $p < 0.001$). Boxes range from the first to the third quartile, whiskers extend to 95% confidence intervals, median is indicated by a line across the box, and mean is indicated by a square marker.

2.2.3 Data Collection and Analysis

All participants underwent a blinded assessment of motor symptom severity using the Movement Disorder Society Unified Parkinson's Disease Rating Scale (MDS-UPDRS) Part III evaluation. This data, as well as demographic data, were stored and managed

using REDCap electronic data capture tools (Harris et al., 2009). Quantitative measures of rigidity were obtained used a custom-built robotic manipulandum (Entact Robotics Inc., Toronto, CA, Figure 2A). The device passively imposed sinusoidal movements of the forearm about the pronation-supination axis through a ± 40° range of motion at 1.5 Hz while measuring the angular displacement and resistive torque required to move the limb. Data was collected using a 1401 data acquisition interface paired with Signal software (Cambridge Electronic Design, Ltd., Cambridge, UK) at a sampling rate of 2000 Hz. Trials were collected separately on the right and left sides, with or without an activation maneuver (tapping the contralateral hand on the leg), a technique that is used clinically to elicit or enhance rigidity. In individuals with mild PD, rigidity can often only be detected during an activation maneuver. Each trial was 45 seconds long. Calculation of rigidity measures was performed using custom MATLAB software (MathWorks, Natick, MA, USA). Four primary measures of rigidity were calculated from the torque, angular displacement, and time data collected by the robotic manipulandum:

1. Angular impulse – a 1st order regression line was fit to the rectified torque data, and the slope of that line was used as the measure of angular impulse (Figure 2C).
   $I = \ slope \int_5^{35} |\tau| \, dt$
2. Peak negative power – the average peak negative power, calculated as the product of torque and angular velocity (derived from displacement) (Figure 2B "Power", arrow). Final value is the average of 30 cycles.
   $$P = \tau \frac{d\theta}{dt}$$
3. Negative work – the integral of negative power (Figure 2B "Power", shaded region).
   $$W = \int_5^{35} P \, dt \, , \qquad P < 0$$
4. Stiffness – the slope of the torque vs. displacement (Figure 2D).
   $$S = \ slope \left(\frac{\tau}{\theta}\right)$$

All measures were calculated using 30 seconds of each trial, discarding the first 5 seconds to allow for stabilization of the imposed trajectory. Torque signals were filtered using a 4^{th} order lowpass Butterworth filter with a 20 Hz cutoff frequency.

Angular impulse, stiffness, and work are rigidity metrics previously used in the literature that correlate well with clinical ratings (Fung, Burne, & Morris, 2000; Patrick, Denington, Gauthier, Gillard, & Prochazka, 2001; Perera et al., 2019; Prochazka et al., 1997). Peak negative power is a unique measure that we implemented in order to address concerns related to the possibility of voluntary movements impacting the validity of our quantitative rigidity measures. Peak negative power represents the maximal rate of negative work done (energy absorption) when the resistive torque of the forearm opposes the direction of the angular velocity. Positive power occurs when the torque and angular velocity are the same direction and may reflect output during which the participant is actively assisting the motion of the robot arm. For this reason, negative power was used to specifically exclude periods of time when the participant may have been actively driving the manipulandum.

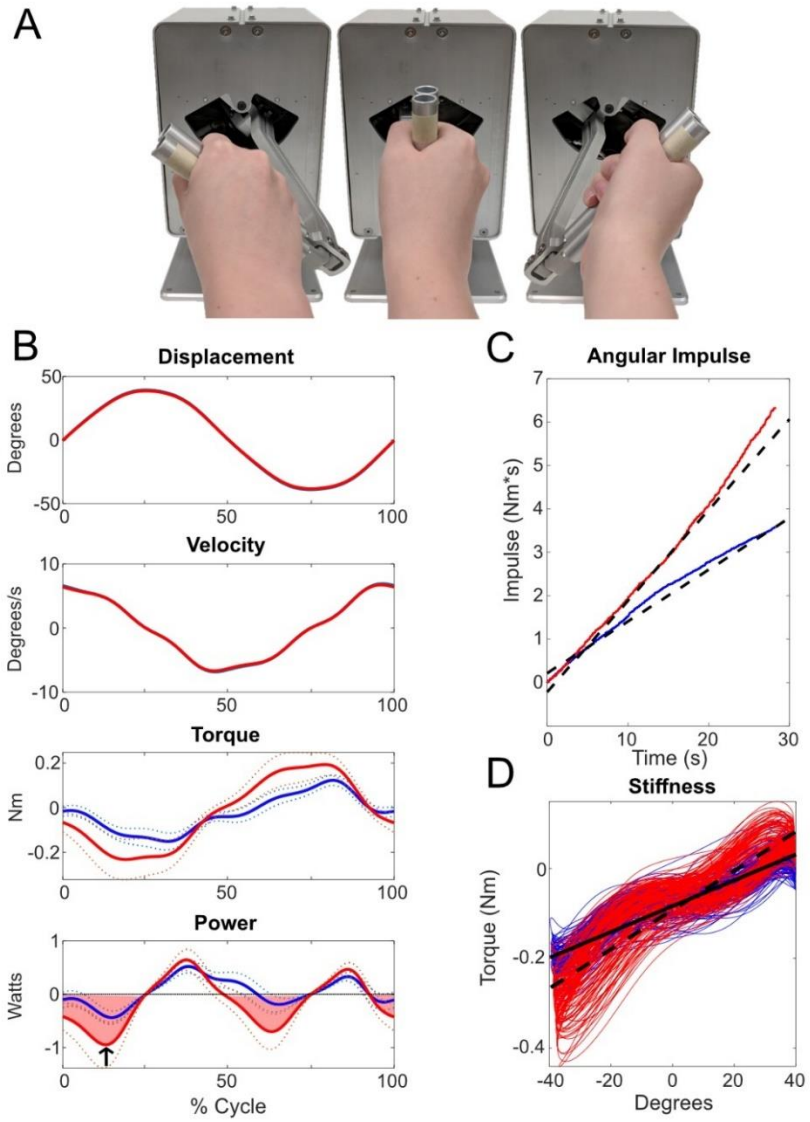

Figure 2. Robotic manipulandum and quantitative rigidity metrics from a single subject. (A) The robotic manipulandum demonstrating approximate pronation, neutral, and supination positions (left to right, respectively). Participants were instructed to hold the handle as the motor rotated the forearm through ± 40 degrees of pronation/supination. Resistive torque was measured through a strain gage attached to the motor. (B-D) Quantitative metrics are shown from two 45 second trials, with higher levels of torque measured during the trial shown in red due to the use of an activation maneuver. (B) Plots showing one cycle of displacement and torque, measured from the robotic manipulandum, as well as velocity and power, which are calculated based on the displacement and torque. In the torque and power plots, the solid line shows the mean values with the standard deviation shown by the dotted lines. The shaded region of the power plot represents the negative work measure. The arrow indicates the peak negative power measure for this cycle. (C) Red and blue lines show integrated torque over time, or impulse. The 1st order regression lines are indicated by the black dashed lines. The slope of the dashed line was used as a measure of angular impulse. D) The slope versus displacement plots are shown in red and blue. The slope of the 1st order regression lines (solid for blue, dotted for red) gives the measure of stiffness.

2.2.4 Statistical Analysis

Demographic features (age, disease duration, MDS-UPDRS Part III total score and rigidity subscore) were compared between groups using a one-way ANOVA (age), t-test (disease duration, levodopa daily equivalent) or an independent samples Kruskal-Wallis test (MDS-UPDRS III total score and rigidity subscore). MDS-UPDRS III upper limb rigidity subscores were compared between sides (more vs. less affected) using a Wilcoxon signed-rank test. Post hoc comparisons were Bonferroni corrected. Spearman's rank correlation coefficients were calculated to assess the correlation between quantitative rigidity measures (without an activation maneuver) and clinical scores of rigidity (MDS-UPDRS III upper limb rigidity subscores) for all participants with PD. The distribution of the quantitative rigidity outcome measures (angular impulse, peak negative power, negative work, stiffness) across subjects (particularly in the PD-RSWA+ group) had an upward skew toward higher rigidity values and did not meet assumptions for normality (Shapiro-Wilk test) or homogeneity of variance (Levene's test). For this reason, data were logarithmically ($\log_{10}$) transformed to achieve a normal distribution. A mixed model ANOVA was run to test for main effects of group (PD-RSWA+, PD-RSWA-, controls), side (more vs. less affected), activation condition (passive vs. with contralateral activation) and interactions between group x side, group x activation, and group x side x activation condition. The primary hypotheses were tested using planned comparisons of rigidity magnitude and symmetry (differences in measures between the more and less affected sides) between groups. In the PD groups, the more and less affected sides were determined by comparing the lateralized scores of the MDS-UPDRS III, which were calculated by summing the scores of all right-side symptoms and left-side symptoms separately. In the control participants, sides were randomly assigned to group 1 or 2 in order to match the distribution seen in the PD participants. Planned comparisons were conducted using Tukey's Honest Significant Difference test. Interaction effects were further explored using post hoc pairwise comparisons, which were Bonferroni corrected. The significance level for all tests was set at $\alpha = 0.05$. Statistical analysis was performed using IBM SPSS 25 (IBM Corp., Armonk, NY, USA).

2.3 Results

2.3.1 Clinical Measures

There were no significant differences in age between the three groups or disease duration between PD groups. However, the levodopa daily equivalent (LDE) was significantly different between the PD groups, with the PD-RSWA+ group having higher LDE than the PD-RSWA- group ($p=0.009$). The MDS-UPDRS Part III total score and rigidity subscore showed a significant effect of group ($p < 0.001$), with both scores significantly higher in both PD groups compared to controls ($p < 0.001$), but there was no significant difference in total scores or rigidity subscores between the PD-RSWA+ and PD-RSWA- groups. Upper limb rigidity subscores were compared between the more and less affected side for each group. There was no significant difference in scores between limb sides in controls. There was a significant difference in upper limb rigidity subscores between the more and less affected limbs in both the PD-RSWA- ($p = 0.001$) and PD-RSWA+ ($p = 0.008$) groups.

Correlations between all four quantitative measures and the MDS-UPDRS III upper limb rigidity subscores were significant ($p < 0.001$) with Spearman's rho values as follows: angular impulse, $\rho = 0.489$; peak negative power, $\rho = 0.532$; negative work, $\rho = 0.441$; and stiffness, $\rho = 0.518$.

2.3.2 Quantitative Rigidity Measures

For all four quantitative rigidity measures (angular impulse, peak negative power, negative work, and stiffness) the mixed model ANOVA revealed significant main effects of group ($F(2,58) > 4.0$, $p < 0.023$), side ($F(1,58) > 8.2$, $p < 0.006$), and activation condition ($F(1,58) > 33.5$, $p < 0.001$). A significant group x side interaction ($F(2,58) > 3.7$, $p < 0.030$) was shown for measures of peak negative power, negative work, and stiffness, while a group x activation condition interaction was significant ($F(2,58) > 3.8$,$p < 0.029$) for measures of angular impulse, peak negative power, and stiffness. Comprehensive results of this analysis are shown in Table 2, and an example plot of peak negative power values is shown in Figure 3.

Table 2. Mixed ANOVA Results. F-statistics and p-values are shown for main effects and interactions analyzed for each quantitative rigidity metric. Significant effects ($p < 0.05$) are indicated with an asterisk. Results of post hoc testing are described in the right column. Participants who exhibited rapid eye movement sleep without atonia (RSWA) in at least one muscle group were categorized as Parkinson's disease with RSWA (PD-RSWA+) while those with no RSWA were categorized as Parkinson's disease without RSWA (PD-RSWA-).

	Main effect of Group	Main effect of Side	Main effect of Activation	Interaction of Group x Side	Interaction of Group x Activation	Post hoc comparisons
Angular impulse	F=4.32, p=0.018*	F=9.86, p=0.003*	F=33.11, p<0.001*	F=2.76, p=0.072	F=4.78, p=0.012*	Group: PD-RSWA+ > Controls Side: More affected > less affected Activation: Activation > no activation Group x Activation: Activation > no activation in PD
Peak negative power	F=4.31, p=0.018*	F=14.59, p<0.001*	F=47.08, p<0.001*	F=4.61, p=0.014*	F=3.75, p=0.029*	Group: PD-RSWA+ > Controls Side: More affected > less affected Activation: Activation > no activation Group x Side: More affected > less affected in PD Group x Activation: Activation > no activation in PD
Negative work	F=4.03, p=0.023*	F=8.24, p=0.006*	F=33.48, p<0.001*	F=3.74, p=0.03*	F=2.59, p=0.084	Group: PD-RSWA+ > Controls Side: More affected > less affected Activation: Activation > no activation Group x Side: More affected > less affected in PD
Stiffness	F=4.68, p=0.013*	F=10.59, p=0.002*	F=33.2, p<0.001*	F=6.88, p=0.002*	F=5.69, p=0.006*	Group: PD-RSWA+ > Controls Side: More affected > less affected Activation: Activation > no activation Group x Side: More affected > less affected in PD-RSWA- Group x Activation: Activation > no activation in PD

2.3.2.1 Difference between groups in rigidity magnitude

Comparisons between groups showed that rigidity scores were significantly higher in the PD-RSWA+ group than in controls ($p < 0.015$) for all rigidity measures. When the more and less affected sides were analyzed separately, peak negative power, negative work, and forearm stiffness were significantly increased in the PD-RSWA+ group compared with controls for all sides and conditions ($p < 0.033$), with the exception of the less affected arm without an activation maneuver. The impulse slope measure was also significantly increased in the PD-RSWA+ group compared with controls in both the more and less affected arms during the activation maneuver condition ($p < 0.013$). In contrast, significant differences in forearm rigidity between the PD-RSWA- and control group were only observed in the more affected limb during the activation maneuver condition ($p < 0.027$). Forearm stiffness was significantly higher in the PD-RSWA+ compared with the PD-RSWA- group in the less affected arm during both activation conditions ($p < 0.045$).

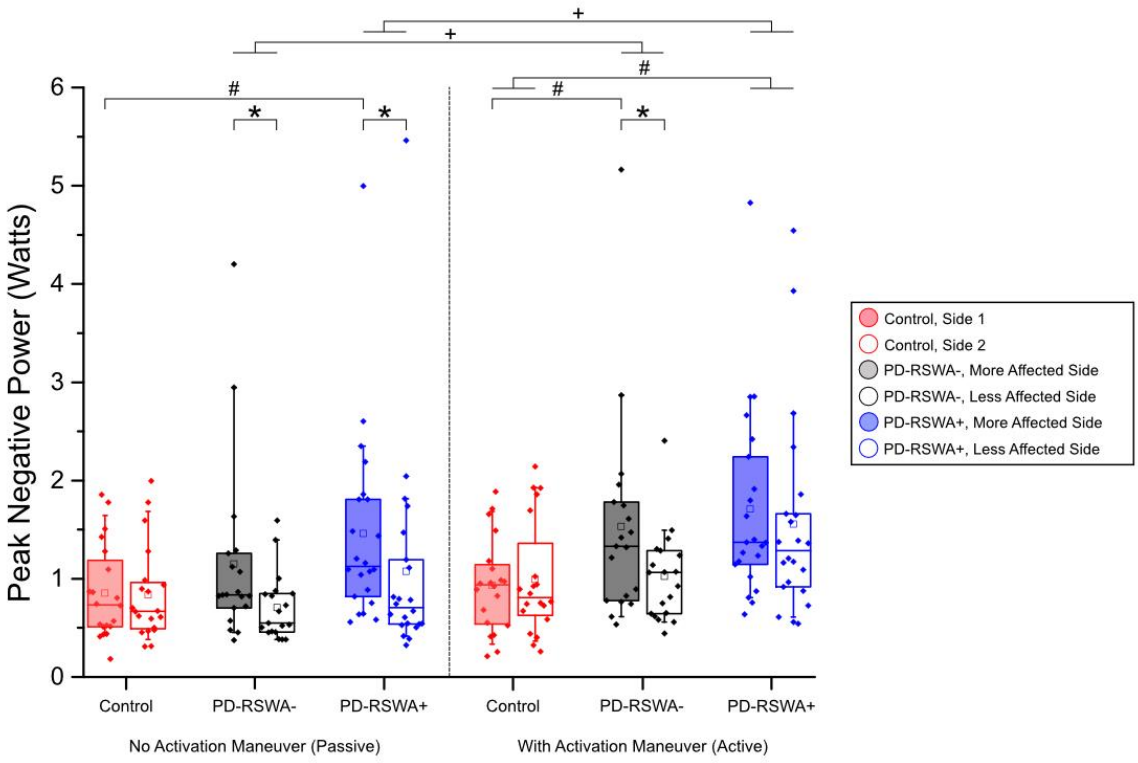

Figure 3. Peak negative power scores for all conditions. Scores for the more (shaded) and less affected limbs are shown for each group, with scores measured without an activation maneuver on the left and scores measured with an activation maneuver on the right. Left and right limbs in the control group were randomly assigned to Side 1 or Side 2 in order to match the distribution of left and right limbs in the more and less affected categories for participants with Parkinson's disease. Data presented in the box plots are original, untransformed data. Statistical significance was determined using a mixed ANOVA of log transformed data, with Bonferroni corrected post hoc pairwise comparisons. Significant between group differences (# $p < 0.027$), within group differences between the more and less affected sides (* $p < 0.008$), and within group differences between the activation maneuver conditions (+$p < 0.001$) are indicated with significance bars. Participants who exhibited rapid eye movement sleep without atonia (RSWA) in at least one muscle group were categorized as Parkinson's disease with RSWA (PD-RSWA+) while those with no RSWA were categorized as Parkinson's disease without RSWA (PD-RSWA). Boxes range from the first to the third quartile, whiskers extend to 90% confidence intervals, median is indicated by a line across the box, and mean is indicated by a square marker. Individual data points are indicated with diamonds.

2.3.2.2 Rigidity symmetry between limbs

The main effect of side indicated that the more affected limb was significantly more rigid than the less affected limb for all four quantitative measures. Analyses of the group x side interaction revealed that there was a significant difference in rigidity scores between the more and less affected sides in the PD-RSWA- group for both the passive

and activation maneuver conditions ($p < 0.028$). In the PD-RSWA+ group, there was a significant difference between sides only for the passive (no activation maneuver) condition ($p < 0.022$). There was no significant difference between sides in the control group for any condition. Planned between-group comparisons of rigidity score symmetry for each quantitative measure (more affected side score – less affected side score) were also performed. Rigidity scores measured without an activation maneuver showed no significant differences in symmetry between the PD-RSWA- and PD-RSWA+ groups or between the control and PD-RSWA+ groups. There was a significant difference in symmetry between the control and PD-RSWA- groups for measures of stiffness and negative work ($p < 0.046$), with the PD-RSWA- group showing greater asymmetry. With the activation maneuver, rigidity score symmetry was significantly different between the control and PD-RSWA- groups for all quantitative measures ($p < 0.033$), with the PD-RSWA- group showing greater asymmetry than controls. There was also a significant difference in symmetry between the PD-RSWA- and PD-RSWA+ groups ($p < 0.039$) for measures of angular impulse and stiffness, with the PD-RSWA- group showing greater asymmetry. There were no significant differences between the control and PD-RSWA+ group symmetry scores with the activation maneuver. Symmetry scores for stiffness are shown in Figure 4.

2.3.2.3 Enhancement of rigidity with an activation maneuver

The main effect of the activation condition showed that rigidity scores for all four outcome measures were significantly higher with an activation maneuver ($p < 0.001$). Post hoc analyses of the group x activation condition interaction found significantly higher rigidity scores for both PD groups on both sides with activation when compared to the no activation condition ($p < 0.015$). There was no significant difference between activation conditions for the control group.

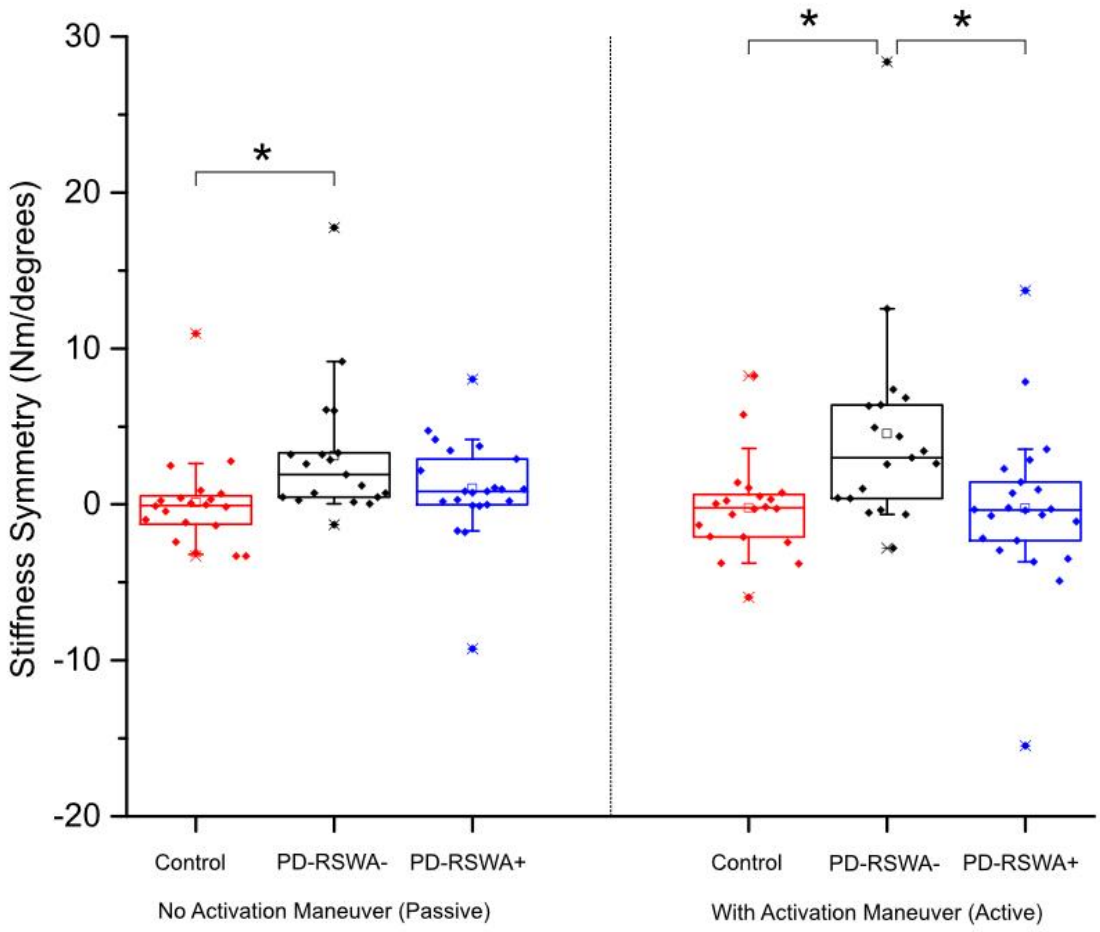

Figure 4. Symmetry scores for the stiffness measure. Symmetry scores were determined by subtracting the quantitative rigidity measure of the less affected limb from the more affected limb, thus values closest to zero indicate the greatest symmetry. Symmetry scores were significantly higher in the Parkinson's disease without RSWA (PD-RSWA) group compared to the control group (Tukey's Honestly Significant Difference test, * $p = 0.031$) in the no activation maneuver condition. In the condition with an activation maneuver, the PD-RSWA group had significantly higher symmetry scores than both the Parkinson's disease with RSWA (PD-RSWA+) and control groups (Tukey's Honestly Significant Difference test, * $p < 0.018$). Boxes range from the first to the third quartile, whiskers extend to 90% confidence intervals, median is indicated by a line across the box, and mean is indicated by a square marker. Individual data points are indicated with diamonds. RSWA: REM sleep without atonia.

2.3 Discussion

There were two main findings from this experiment. First, measures of forearm rigidity were significantly increased in the PD-RSWA+ group compared to control subjects. In contrast, significant differences in forearm rigidity between the PD-RSWA- and control group were only observed in the more affected limb during the activation maneuver condition. Second, asymmetry in the expression of forearm rigidity (calculated

as the difference in quantitative scores between the more and less affected sides) was higher in the PD group without RSWA (PD-RSWA-) relative to controls and, for some variables, more asymmetric than the PD-RSWA+ group, particularly with the use of an activation maneuver. There were no significant differences in asymmetry between controls and the PD-RSWA+ group. These findings demonstrate that the loss of atonia during REM sleep is associated with increased bilateral expression of forearm rigidity in people with PD.

Two primary, albeit not mutually exclusive, explanations might account for the increased rigidity in the cohort with early PD and RSWA. First, increased expression and symmetry of rigidity may reflect increased disease severity and more extensive degeneration of nigrostriatal dopaminergic neurons bilaterally. Rigidity increases in severity as PD progresses, and in individuals with akinetic-rigid predominant PD, rigidity progresses faster than in the tremor predominant subtype (Vu et al., 2012). In addition, motor signs, including rigidity, typically become more symmetrical with disease progression (Marinus & van Hilten, 2015). This explanation aligns with previous work suggesting that the co-expression of idiopathic RBD and PD is associated with increased severity and faster disease progression (Chahine et al., 2014; Folle et al., 2019). In the present study, there was no significant statistical difference in age or disease duration between the PD groups. However, the disease duration was longer (on average by 0.7 years) and disease severity was worse in the RSWA+ group (on average by 5 points on the MDS-UPDRS Part III). Given the inherent inaccuracies of estimating disease duration based on time since diagnosis or time from first symptoms, we cannot rule out the possibility that the PD-RSWA+ group has had a longer disease duration thus providing more time to manifest increases in bilateral rigidity.

A second possibility is that increased expression of symmetric rigidity in the PD-RSWA+ participants may be mediated by the early degeneration of brainstem structures that contribute to the regulation of muscle tone. The circuits responsible for the control of REM sleep muscle tone involve multiple interconnected brainstem nuclei (B. F. Boeve et al., 2007). Portions of this circuit overlap with nuclei that contribute to spinal motor neuron excitability, postural control, and locomotion during wakefulness, such as the pedunculopontine nucleus, pontomedullary reticular formation, locus coeruleus and

caudal raphe nucleus. Degeneration in nuclei that control REM sleep muscle tone (e.g. sublaterodorsal nucleus) likely precedes the loss of neurons that contribute to alterations in muscle tone regulation during wakefulness such as the locus coeruleus, caudal raphe, magnocellular and gigantocellular reticular formation (Braak Stage 2) and the pedunculopontine nucleus (Braak stage 3) (B. F. Boeve et al., 2007; Braak et al., 2006, 2003). This may explain why overt signs of rigidity are not expressed until 3-5 years prior to a diagnosis of PD in people with idiopathic RBD (Fereshtehnejad et al., 2019).

It has been hypothesized that parkinsonian rigidity may be driven, in part, by dysfunctional reticulospinal tract output originating in the nucleus reticularis giganto cellularis (NRGc) (Delwaide, 2001). Caudal regions of the pedunculopontine nucleus send cholinergic projections to both the NRGc and ventromedial medullary reticular formation (Martinez-Gonzalez, Bolam, & Mena-Segovia, 2011). Reticulospinal neurons in these regions project bilaterally to the spinal cord and can influence muscle tone via direct and indirect connections to alpha and gamma motoneurons in the spinal cord (Carpenter, 1991; C D MacKinnon, 2018). Accordingly, the symmetrical expression of rigidity may reflect disordered control of motor neuron excitability due to pedunculopontine nucleus and/or reticular formation pathology. In keeping with this idea, Bliwise et al. showed that elevated phasic muscle activity during REM sleep is associated with a more symmetric presentation of disease in a cohort with comparable disease duration (Bliwise et al., 2010).

Early development of synucleinopathy in the locus coeruleus and caudal regions of the raphe nucleus (Braak et al., 2006) may also contribute to changes in spinal motoneuron excitability during wakefulness. The locus coeruleus and raphe nucleus send extensive noradrenergic and serotonergic projections to motor neurons in the spinal cord. These inputs play a critical role in the modulation of motor neuron firing by amplifying and prolonging synaptic input and facilitating self-sustained firing through the induction of persistent inward currents (Heckman, Gorassini, & Bennett, 2005; Heckman, Mottram, Quinlan, Theiss, & Schuster, 2009). Persistent inward currents allow the motor neuron to continue firing in the absence of synaptic input. These mechanisms are considered to play an important role in postural control by reducing the need for sustained synaptic input.

Accordingly, reduced descending input from this system could result in disordered control of motor neuron firing in response to sensory afferent or descending input.

The mechanisms contributing to the expression of rigidity are poorly understood but alterations in the excitability of both cortical and subcortical pathways mediating long-latency stretch reflexes (Rothwell et al., 1983; Tatton & Lee, 1975) and stretch induced co-activation of agonist-antagonist (R Xia et al., 2006; Ruiping Xia, 2011; Ruiping Xia & Rymer, 2004; Ruiping Xia et al., 2009) have been proposed. Early studies of rigidity pathophysiology identified that the long-latency component of the stretch reflex evoked by rapidly imposed displacements of the upper limb was abnormally enhanced in PD (Berardelli et al., 1983; Mortimer & Webster, 1979; Rothwell et al., 1983; Tatton & Lee, 1975). In the hand and wrist muscles, the long-latency stretch reflex occurs after the spinally mediated short-latency stretch reflex and is thought to be mediated, in part, by a polysynaptic transcortical pathway via the primary motor cortex (Angel & Lemon, 1975; Cheney & Fetz, 1984; Colum D. MacKinnon et al., 2000; Matthews, 1991). In more proximal muscles, subcortical structures are considered to play more of a role in the generation of long latency responses to imposed stretch (F. A. Lenz, Tatton, & Tasker, 1983; F. Lenz, Tatton, & Tasker, 1983). Thus, changes in sensorimotor processing at the cortical or subcortical level may contribute to the expression of rigidity in the forearm during passively imposed movements. In addition to abnormally enhanced long-latency reflexes, people with PD may also show an abnormal shortening reaction, defined as an increase in activity in muscles shortened by an imposed movement (Berardelli et al., 1983; Ruiping Xia & Rymer, 2004). The shortening reaction leads to co-contraction and increased joint stiffness during passive movement. The mechanisms mediating the shortening reaction in PD are poorly understood but changes in the pathways controlling short-latency autogenic inhibition, suggesting abnormalities in the excitability of Ia and Ib spinal interneurons, may contribute (Delwaide et al., 1991). These populations of interneurons are modulated by inputs from the reticulospinal tract, again suggesting that dysfunction of reticular nuclei may contribute to the expression of rigidity (Delwaide, 2001; Delwaide, Pepin, De Pasqua, & Maertens de Noordhout, 2000). Taken together, it is likely that all of the above mechanisms contribute and interact to increase muscle activity during imposed movements (Ruiping Xia et al., 2009), but

expression of rigidity may be dependent upon location and extent of cortical or subcortical degeneration for a given individual. Our data shows that rigidity is increased bilaterally in people with PD and RSWA, which could suggest increased involvement of subcortical pathways.

Contralateral movements used as an activation maneuver resulted in a significant increase in rigidity in both PD groups but not in control subjects. This finding is consistent with previous studies (Fung et al., 2000; Hong, Perlmutter, & Earhart, 2007; Powell, Hanson, Joseph Threlkeld, Fang, & Xia, 2011) and further supports and validates the use of the contralateral activation maneuver as a method to differentiate between healthy adults and people with parkinsonism. The relative increase in rigidity evoked by activation was substantially higher in the PD-RSWA- (55%) compared with the PD-RSWA+ group (15%), and enhanced the symmetric presentation of symptoms in the PD-RSWA+ group. The increased symmetry may be due to a ceiling effect, such that the rigidity in the PD-RSWA+ group's more affected limb can only increase a small amount with activation, whereas the PD-RSWA- shows a large increase in rigidity in both limbs. Currently, the mechanisms mediating the increase in rigidity when contralateral movements are performed are poorly understood. Assuming that rigidity is mediated in part by a transcortical long-latency stretch reflex, it is possible that the activation maneuver enhances this reflex through changes in cortical activity. Isometric muscle contractions as well as rhythmic movements of the upper limb have been shown to increase cortical excitability of the ipsilateral motor cortex (Carson et al., 2004; Hortobágyi, Taylor, Petersen, Russell, & Gandevia, 2003), which suggests a possible mechanism for the activation maneuver. Changes in spinal motoneuron excitability via crossed sensory afferent feedback (e.g. group lb for the activation side) may increase the sensitivity to imposed stretch or impact of the shortening reaction on measures of rigidity (Powell et al., 2011). Alternatively, the activation maneuver may facilitate bilateral descending projects from regions of the reticular formation that regular muscle tone and stretch reflex gain.

2.4 Conclusions

Our findings confirm that people with PD and RSWA have unique dysfunction in the regulation of muscle tone during both sleep and wakefulness. They also suggest that RSWA in the setting of PD predicts distinctive brain stem neuropathology. These discoveries are fundamentally important because they help investigators understand the physiology of motor activity and the pathophysiology of Parkinsonian disorders. To our knowledge, this is the first study to use quantitative measures to compare the level and bilateral expression of rigidity between people with PD with and without RSWA. While previous studies have found increased symptom severity in individuals with PD and idiopathic RBD, our study shows that even in mild to moderate PD, the presence of RSWA (even without a diagnosis of idiopathic RBD) is associated with increased rigidity magnitude and symmetry, especially upon use of an activation maneuver. It remains unclear whether the increased expression of rigidity reflects increased disease severity or increased involvement of subcortical pathways.

CHAPTER 3 PATHWAY ACTIVATION DIFFERS BETWEEN DORSAL AND VENTRAL DEEP BRAIN STIMULATION OF GLOBUS PALLIDUS

Maria Linn-Evans, Sommer Amundsen Huffmaster, Emily Lecy, Angela Noecker, Cameron McIntyre, Tara Palnitkar, Remi Patriat, Noam Harel, Matthew Johnson, Colum MacKinnon

3.1 Introduction

Deep brain stimulation (DBS) is a neuromodulation-based therapy that has been approved for use in Parkinson's disease (PD) for nearly 20 years. DBS provides clinically meaningful improvements in cardinal motor symptoms for the majority of patients, but there still remains a great deal of heterogeneity in responses to DBS as evidenced by reported average improvement in MDS-UPDRS motor scores ranging from 11 – 70% (Weaver et al., 2005). Both subthalamic nucleus (STN) and globus pallidus (GP) are approved as targets for DBS in individuals with PD and multiple studies have shown that DBS in these regions is equally effective in mitigating dopaminergic-responsive

symptoms of PD such as tremor, bradykinesia, and rigidity (Anderson, Burchiel, Hogarth, Favre, & Hammerstad, 2005; Follett et al., 2010; Odekerken et al., 2013). However, not all symptoms respond favorably to DBS. Cognitive decline, impairment in speech and swallowing, and gait and balance dysfunction can often worsen after STN-DBS or GP-DBS (Weaver et al., 2012). Despite the comparable efficacy of STN and GP-DBS, STN-DBS is currently the preferred target at the majority of neurosurgical centers. As a result, less is known about GP as a target for DBS, but there is some evidence that GP-DBS may have distinct advantages over STN-DBS. Compared to STN-DBS, GP-DBS is less likely to cause cognitive side effects, provides better dyskinesia suppression, and can be easier to program, making it an appealing option for many patients and clinicians (Williams et al., 2014). Unfortunately, there is significant variability in outcomes for patients due to many factors including lead location, individual anatomy, patient phenotype, and programming parameters. In order to improve the efficacy of GP-DBS, it is crucial to develop an understanding of the relationship between stimulation location and the improvement or worsening of symptoms and identify the neural structures and pathways responsible for mediating these effects.

When performing GP-DBS surgery, surgeons typically target the anterolateral part of the motor territory of the globus pallidus internus (GPi), near the border of the globus pallidus externus (GPe) (Starr, 2002). Within GPi, the motor territory occupies the posterolateral region of the nucleus, with some variation between individuals (Patriat et al., 2018). The anterolateral portion of the motor territory is often selected as the target so the stimulation can spread throughout most of the motor territory of the GPi, without spreading to the internal capsule, which sits 3-4 mm medial to the target. The standard lead trajectory into GPi is 60° from the anterior commissure to posterior commissure line in the sagittal projection, and 0° lateral from the vertical in the coronal projection (Starr, 2002). Although this standard GP-DBS target is effective for many patients, an important consideration for GP-DBS is the seemingly opposite effects of stimulation between the ventral and dorsal regions of GP. Stimulation of dorsal areas of sensorimotor GPi (or ventral regions of GPe) can greatly reduce akinesia while leading to worsening of dyskinesias, while stimulation of ventral GPi suppresses dyskinesias but can worsen akinesia and gait (P. Krack et al., 1998; Vitek, Hashimoto, Peoples, DeLong, & Bakay,

2004; Yelnik et al., 2000). These location-dependent effects of stimulation within GP are likely due to the activation of specific projections that have opposite downstream effects on the motor system. Early studies suggested that the opposite effects may be mediated by the lenticular fasciculus, which was thought to have more axons passing through the dorsal GPi, and ansa lenticularis which had more axons in ventral GPi (P. Krack et al., 1998). However, this hypothesis was based on a lesion-based understanding of DBS where stimulation of a pathway was thought to block neural activity. The current understanding of DBS focuses on an activation-based mechanism, where DBS drives axonal activity that helps modulate neural patterns into a more regular state (M. D. Johnson et al., 2008). Based on this mechanism of DBS, a more likely hypothesis is that stimulation of dorsal GPi leads to preferential activation of GPe efferents that inhibit activity in GPi and STN (Vitek et al., 2004; Vitek, Zhang, Hashimoto, Russo, & Baker, 2012), while ventral stimulation preferentially activates pallidothalamic projections and the inhibits the pedunculopontine nucleus (PPN) (Jianyu Zhang, Wang, Baker, & Vitek, 2012). Understanding the relationship between the stimulation location, pathway activation, and the effects on motor signs would allow for GP-DBS to be programmed based on individual patient needs. Additionally, it is possible that there is an ideal region for stimulation in GP that balances the need for dyskinesia suppression with reductions in akinesia and gait dysfunction.

One tool that has great potential for improving the understanding of GP-DBS and thus patient outcomes is computational modeling of DBS. In this study, we use high-field 7T magnetic resonance imaging (MRI) to extract precise patient-specific anatomy, finite element models to estimate voltage distribution, and the gold-standard multi-compartment cable model of axons to account for the electrical and biophysical properties of human axons. The aim of this study was to develop state-of-the-art patient-specific computational models of pallidal DBS and estimate the activation of pathways with stimulation in either the ventral or dorsal region of GPi. We expected dorsal stimulation to lead to preferential activation of GPe projections to GPi and STN, and ventral stimulation to preferentially activate pallidothalamic projections.

3.2 Methods

3.2.1 Participants

Nine individuals (3 women, 6 men, age = 62.8 ± 8.6) with Parkinson's disease participated in this study (Table 3). Inclusion criteria were diagnosis of idiopathic Parkinson's disease by a movement disorders neurologist, existing deep brain stimulation system implanted in globus pallidus, and presence of pre-surgical 7T MRI and post-surgical computed tomography (CT) scans. Individuals were excluded from the study if they had a history of musculoskeletal disorders affecting movements of the limbs, neurological disorders besides PD, history of dementia or cognitive impairment, or post-operative complications that could affect patient safety or confound experimental results. All study procedures were approved by the University of Minnesota Institutional Review Board and all participants provided written informed consent according to the Declaration of Helsinki.

Table 3. Demographics of study participants. Movement Disorder Society Unified Parkinson's Disease Rating Scale III (MDS-UPDRS III) was performed OFF medication and OFF stimulation. Levodopa daily equivalent (LDE) was determined based on the Tomlinson formula (Tomlinson et al., 2010). DBS = Deep brain stimulation

ID	Sex	Age	Years since diagnosis	MDS-UPDRS III	LDE (mg)	Implant Side	DBS Device
UD1001	M	53	15	56	696	Bilateral	Medtronic Activa
UD1002	M	56	11	43	1010	Bilateral	Medtronic Activa
UD1005	F	82	11	50	825	Right	Abbott Infinity
UD1013	M	71	8	48	950	Left	Medtronic Activa
UD1015	F	63	5	66	800	Bilateral	Abbott Infinity
UD1018	F	60	9	51	1000	Right	Abbott Infinity
UD1022	M	62	11	67	150	Bilateral	Abbott Infinity
UD1032	M	64	9	67	800	Bilateral	Medtronic Activa
UD1034	M	54	5	52	850	Bilateral	Medtronic Activa

3.2.2 Imaging

Prior to DBS surgery, all participants underwent a 7T MRI at the Center for Magnetic Resonance Research at the University of Minnesota using a Siemens console, SC72 gradient coil, and 32-channel head coil. The imaging protocol included high-resolution anatomical scans (T1 and T2 weighted) as well as diffusion weighted imaging (DWI) using protocols which have been described in previous publications (Abosch, Yacoub, Ugurbil, & Harel, 2010; Duchin, Abosch, Yacoub, Sapiro, & Harel, 2012; Lenglet et al., 2012). One month following surgery, participants underwent a routine clinical CT scan, which was registered with the T1-weighted MRI to allow for lead localization.

Pre-processing corrections were performed to address image distortions inherent in this imaging pipeline. For the T1-weighted anatomical images, this included corrections for non-uniformity using FSL FAST (Woolrich et al., 2009), brain extraction with FSL BET (Smith, 2002), and co-registrations with T2-weighted images using FSL FLIRT with 6 degrees-of-freedom followed by a 12 degrees-of-freedom registration in order to make fine adjustments (Jenkinson & Smith, 2001). For the DWI, FSL TOPUP was used to correct susceptibility-induced distortions (Andersson, Skare, & Ashburner, 2003). Additionally, anatomical and DWI images were co-registered. Manual segmentations of basal ganglia nuclei (globus pallidus externus (GPe), globus pallidus internus (GPi), subthalamic nucleus (STN) and substantia nigra (SN)) were extracted from the T2-weighted anatomical images by research staff experienced in this technique (Duchin et al., 2018).

3.2.3 Experimental Deep Brain Stimulation Settings

The primary goal of this project was to evaluate the relative effects of dorsal versus ventral deep brain stimulation, which required the development of experimental DBS settings for each participant. StimVision, a software tool used to estimate the volume of tissue activated (VTA) by DBS, was used to identify stimulation settings that theoretically biased DBS to either dorsal or ventral aspects of the targeted nucleus (A. M. Noecker et al., 2018).

For each subject, 7T MRI data were used to create an anatomical model of each brain hemisphere (Gunalan et al., 2017). The manually segmented basal ganglia nuclei (GPe, GPi, STN, SN) were constructed into 3D volumes for visualization with the MRI slice data. The T1-weighted MRI was used as the base image for data co-registration, and the patient anatomical model was merged with the post-operative CT image to identify the DBS electrode location in the brain. The patient-specific imaging data, anatomical volumes, and DBS electrode location were loaded into the StimVision software tool to assist with the definition of experimental DBS settings that would be used in the modeling experiments. Volume of tissue activated estimates of stimulation spread were used to guide selection of the contact and amplitude for the model-based DBS setting (Chaturvedi, Luján, & McIntyre, 2013). The pulse width (60 us) and stimulation frequency (130 Hz) were held constant for all DBS settings.

For each brain hemisphere, an expert in DBS modeling blinded to the clinical settings (CCM), used the patient-specific StimVision model to select an electrode contact that most closely fit the anatomical designation of dorsal or ventral placement within the GP. Next, VTA estimates were used to define a stimulation amplitude through the selected electrode contact which fulfilled the following criteria: 1) concentrated stimulation in the targeted anatomical area, 2) avoided stimulation spillover to the non-targeted anatomical area, and 3) avoided stimulation spillover to the internal capsule. Definition of the StimVision experimental DBS settings was blinded to any information about the subjects, aside from the imaging data used to create the patient-specific DBS model. Experimental dorsal and ventral settings are presented in Table 4. The electrodes used for each setting were localized relative to the ventral GPi border using a custom MATLAB script. The distance along the dorsal/ventral axis between the center of the active electrode and the most ventral point of the GPi was calculated for each individual setting. The distances averaged by setting are presented in Table 5 and histograms showing the electrode distributions relative to the ventral GPi border are presented in Figure 5.

Table 4. Experimental deep brain stimulation settings identified using StimVision. Dorsal and ventral settings were developed for each implanted lead based on criteria described in section 3.2.3 Experimental Deep Brain Stimulation Settings. The active contacts are listed under the Dorsal and Ventral Settings columns for each lead. The anode is indicated as a number followed by a $^-$ (e.g. 3^-, indicating that contact 3 is set as the anode). The cathode is indicated with a $^+$ sign. In instances where the case (implanted pulse generator) is set as the cathode, this is abbreviated with a C (e.g. C^+). For settings involving segmented electrode contacts, the active segments are indicated in parentheses following the contact number. After the contact information, the amplitude, frequency, and pulse width are listed.

Subject ID	Lead	Implant Side	Dorsal Settings	Ventral Settings
UD1001	Medtronic 3389	Left	3^-C^+, 3V, 120Hz, 60us	1^-C^+, 3V, 120Hz, 60us
	Medtronic 3387	Right	3^-C^+, 3V, 120Hz, 60us	1^-C^+, 3V, 120Hz, 60us
UD1002	Medtronic 3389	Left	3^-C^+, 2V, 120Hz, 60us	2^-C^+, 2V, 120Hz, 60us
		Right	3^-C^+, 2V, 120Hz, 60us	2^-C^+, 2V, 120Hz, 60us
UD1005	Abbott 6172	Right	4^-C^+, 3mA, 120Hz, 60us	$2(bc)^-C^+$, 3mA, 120Hz, 60us
UD1013	Medtronic 3389	Left	2^-C^+, 2V, 120Hz, 60us	1^-C^+, 2V, 120Hz, 60us
UD1015	Abbott 6172	Left	4^-C^+, 2mA, 120Hz, 60us*	$2(c)^-C^+$, 1mA, 120Hz, 60us
		Right	4^-C^+, 2mA, 120Hz, 60us*	$2(b)^-C^+$, 1mA, 120Hz, 60us
UD1018	Abbott 6172	Right	4^-C^+, 2.5mA, 120Hz, 60us	$2(ab)^-C^+$, 2.5mA, 120Hz, 60us
UD1022	Abbott 6172	Left	$3(b)^-C^+$, 2mA, 120Hz, 60us	$2(b)^-C^+$, 2mA, 120Hz, 60us
		Right	$3(a)^-C^+$, 2mA, 120Hz, 60us	$2(a)^-C^+$, 2mA, 120Hz, 60us
UD1032	Medtronic 3389	Left	3^-C^+, 2V, 120Hz, 60us	2^-C^+, 2V, 120Hz, 60us
		Right	3^-C^+, 2V, 120Hz, 60us	1^-C^+, 2V, 120Hz, 60us
UD1034	Medtronic 3389	Left	2^-C^+, 2V, 120Hz, 60us	0^-C^+, 2V, 120Hz, 60us
		Right	3^-C^+, 2V, 120Hz, 60us	1^-C^+, 2V, 120Hz, 60us

Table 5. Average electrode locations. Average distances between the ventral globus pallidus internus (GPi) border and the active electrode were calculated for the electrodes used in each experimental setting. Distance was measured along the dorsal/ventral axis from the most ventral point of the GPi to the center of the active electrode. Higher values indicate that the electrode is located more dorsally in the nuclei.

Setting	Mean distance ± SD (mm)
Ventral	3.9 ± 1.3
Dorsal	6.5 ±1.5

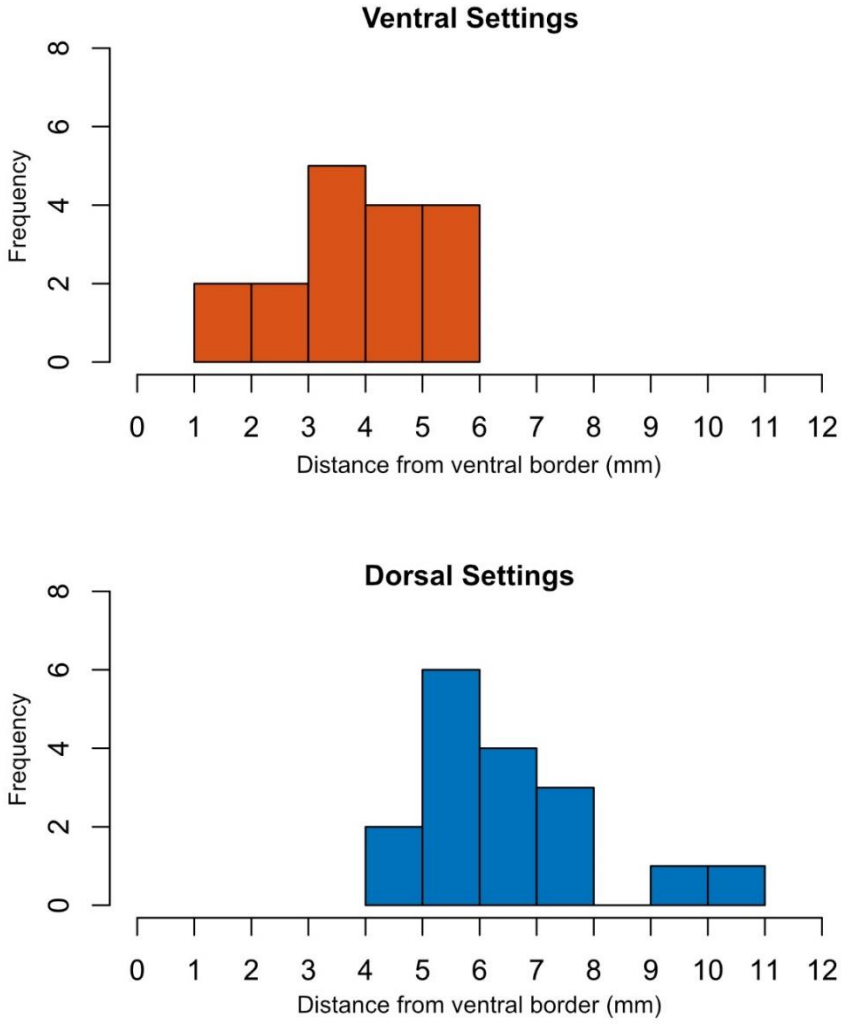

Figure 5. Distribution of electrode locations. Distances between the ventral globus pallidus internus (GPi) border and the active electrode for each experimental setting were calculated along the dorsal/ventral axis. The distribution of electrode locations for each experimental setting type (ventral and dorsal) is presented as a histogram, with the distance in mm along the x-axis and the number of electrodes along the y-axis.

3.2.5 Multi-Compartment Cable Model Axon Trajectories

In order to model the basal ganglia anatomy for each individual, a variety of methods were used to construct axon models of GP projection neurons and other nearby fiber tracts. Nuclei segmented from 7T T2-weighted MRI (GPe, GPi, STN, SN), probabilistic tractography, and descriptive anatomical studies were used to define and model the internal capsule (IC), pallidothalamic (ansa lenticularis (AL) and lenticular fasciculus (LF)), and pallidosubthalamic (GPe→GPi→STN and GPe→STN) pathways for each participant. Two pathways (IC and AL) were reconstructed from the 7T DTI using probabilistic tractography. Fiber orientations were estimated at each voxel using FSL bedpostx with a maximum of 3 crossing fibers. Probabilistic tractography, which approximates the connectivity and three-dimensional shape of fiber tracts by creating streamlines in a probabilistic manner, was run using FSL Probtrackx (Behrens, Berg, Jbabdi, Rushworth, & Woolrich, 2007). The IC was constructed from seed masks in two motor areas, primary motor cortex (M1, Brodmann's area 4) and Brodmann's area 6 (BA6), which contains premotor and supplementary motor areas. The seed masks for M1 and BA6 were acquired using the Freesurfer image analysis suite, and a manually segmented cerebral peduncle mask was used as the waypoint (Fischl, 2012). For the AL, GPi was used as the seed mask and the waypoint mask covered the thalamus. The resulting tractography was manually edited in 3D Slicer to isolate the AL. The LF is difficult to visualize with tractography due to its crossing with the internal capsule, thus the LF was modeled based on a basal ganglia pathway atlas that was manually aligned with the GPi of each individual (Petersen et al., 2019). The pallidosubthalamic pathways were constructed in MATLAB using manually segmented nuclei (GPi, STN, SN) as waypoints for randomly distributed GPe cells that were then connected via a spline fitting algorithm. The percentage of GPe projections passing through GPi (37.5%) vs. travelling directly to STN (62.5%) were determined based on histological studies in non-human primates (Sato, Lavallée, Lévesque, & Parent, 2000). Visualizations of these modeled pathways are shown in Figure 6.

Each of the resulting fiber tracts were populated with multi-compartment cable models of myelinated axons with a fiber diameter of 2 um (Innocenti, Vercelli, & Caminiti, 2014; Liewald, Miller, Logothetis, Wagner, & Schüz, 2014; Mathai et al.,

2013). The multi-compartment axon models consisted of nodes of Ranvier, myelin attachment segments, paranode main segments and internode segments with membrane dynamics consistent with those used in previous studies (M. D. Johnson & McIntyre, 2008; M. D. Johnson, Zhang, Ghosh, McIntyre, & Vitek, 2012; McIntyre, Richardson, & Grill, 2002). The GPi, GPe, and IC were each initially populated with 1000 axons. The starting points for AL axons were restricted to the anterior 1/3 of the GPi and the LF starting points were restricted to the posterior 2/3 to better reflect their reported distribution (Baron, Sidib, Delong, & Smith, 2001). In order to account for axonal damage during lead insertion, axons that intersected with the lead or 0.25 mm thick encapsulation layer were removed from the model. On average, 9% of the lenticular fasciculus neurons, 8% of the GPe→GPi→STN neurons and 5% of the GPe→STN were removed. In one participant (UD1005), a significant lacuna was present in the GP and axons were also removed from this region, resulting in the removal of 32% of AL neurons, 23% of LF neurons, 37% of GPe→GPi—STN neurons and 29% of GPe→STN neurons.

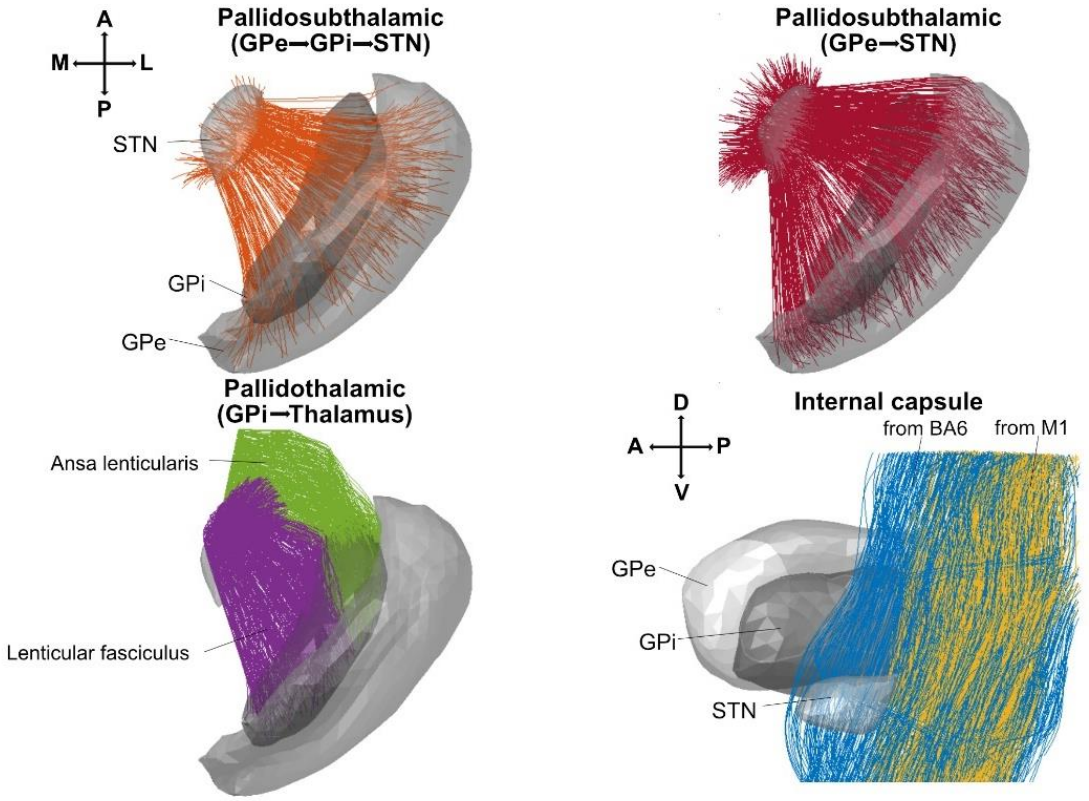

Figure 6. Visualization of modeled axonal pathways. Modeled axonal pathway trajectories are shown relative to the globus pallidus externus and internus (GPe and GPi) and subthalamic nucleus (STN). Six pathways were developed for this computational model: ansa lenticularis, lenticular fasciculus, internal capsule from primary motor cortex (M1), internal capsule from Brodmann's area 6 (BA6), and two pallidosubthalamic tracts, GPe→STN and GPe→GPi→STN. Each structure from which axons projected (GPe, GPi, and motor cortex) was populated with 1,000 axon initiation points.

3.2.4 Finite Element Model

Each participant's DBS lead(s) and imaging-derived brain anatomy were incorporated into a patient-specific finite element model (FEM) built using COMSOL Multiphysics 5.4. To account for varying conductivities within the brain, FSL's FAST tool was used to segment the T1-weighted anatomical images into white matter, grey matter, and cerebrospinal fluid (Jenkinson, Beckmann, Behrens, Woolrich, & Smith, 2012; Y. Zhang, Brady, & Smith, 2001). Any areas outside of the brain but within the skull were considered bulk head tissue. Conductivity tensors were then estimated for each voxel of the participant's DWI and imported into COMSOL to account for inhomogeneity and anisotropy within the brain in the FEM (Howell & McIntyre, 2017; Schmidt & Van Rienen, 2012). The conductivity tensors were calculated based on isotropic electrical properties estimated at the median frequency of the applied stimulus

waveform (3049Hz for current-controlled or 4294Hz for voltage-controlled systems) and the conductivities were set at 0.11 S/m for grey matter and 0.065 S/m for white matter based on models of dielectric properties of various body tissues (Gabriel, Lau, & Gabriel, 1996a, 1996b). The cerebrospinal fluid and bulk head tissue were modeled with isotropic electrical properties (0.3 S/m). Brain surface geometry extracted from the T1-weighted image using FSL BET was smoothed using 3D Slicer's Gaussian smoothing tool and imported as a surface into the model. The DBS lead (Medtronic 3389, Medtronic 3387, or Abbott Infinity 6172), a 0.25 mm thick isotropic (0.3 S/m) encapsulation layer surrounding the lead, and a generic skull profile were also included in the FEM. For current-controlled systems, a normal current density was applied to the active electrode surfaces by dividing a 1 mA pulse amplitude by the surface area of the electrode. For voltage-controlled systems, a 1 V electric potential was applied to the active electrode. The base of the neck was set as ground, while the rest of the head surface and lead shaft had a current density of zero. Simulations were run at a single AC frequency of 3049 Hz or 4294 Hz based on the median frequency of the waveform used for either a current or voltage-controlled device. The finite element analysis was solved using COMSOL's AC/DC module. The extracellular voltages predicted by the FEM were interpolated at each compartment of the multi-compartment cable axon models.

3.2.6 Simulating Axonal Pathway Activation

Stimulation of the modeled axons was performed using NEURON, a programming environment designed for modeling networks of neurons (Hines & Carnevale, 1997). For each participant, a 10-pulse square current-controlled or voltage-controlled waveform was created using the pulse width and frequency of their DBS settings. The waveforms were filtered to best match the properties of a waveform passing through neural tissue (Yousif, Bayford, & Liu, 2008). This waveform was then applied to each compartment of the axonal model and axons were considered "activated" if action potentials were elicited within 3 ms after at least 80% of the pulses. A binary search algorithm was employed to determine the stimulus amplitude threshold (±0.1 mA or V) required to activate each axon at a given stimulation setting. The ratio of active to inactive axons was used to define the percentage of activated axons for each pathway.

Recruitment curves indicating the relationship between the stimulus amplitude and percentage of axons activated were also generated for each pathway.

3.2.7 Model Validation

In order to validate the output of this patient-specific model, the relationship between capsular side effects and model-predicted internal capsule activation was analyzed. Monopolar review documents from each subject were screened for capsular side effects, including: dystonic limb posture, facial muscle contraction, conjugate eye deviation, and dysarthria (Matias et al., 2015). Modeled axons were then stimulated using the settings noted in the monopolar review to determine the percentage of internal capsule axons that were activated. Based on previous studies, activation of 5-15% of internal capsule axons is sufficient to elicit muscle contractions measurable by EMG - in some cases, as little as 1% of internal capsule axons need to be activated in order to elicit contractions (Chaturvedi, Butson, Lempka, Cooper, & McIntyre, 2010).

3.2.8 Comparison of Dorsal and Ventral Experimental Settings

To compare the activation of axonal pathways between the dorsal and ventral experimental settings, paired Wilcoxon Signed Rank tests were used to test for differences in the percentage of axons activated by each setting. In addition to testing differences between the experimental dorsal and ventral settings, recruitment curves were also created for the dorsal and ventral contacts. The recruitment curves show the relationship between an applied voltage or current and the percentage of axons activated in a pathway. To construct the average recruitment curves for this analysis, axonal activation was measured at 0.1 V or mA intervals between 0 and 10 V or mA using the active electrode from either the dorsal or ventral model setting for each subject.

3.3 Results

3.3.1 Model Validation

Seven out of nine subjects (10 out of 15 sides) reported capsular side effects during monopolar review (Table 6). Dysarthria and facial muscle contraction (often described as “pulling”) were the most commonly reported side effects. The percentage of axons activated during the settings resulting in capsular side effects were calculated for internal capsule pathways from primary motor cortex. The mean percent activation of IC

axons was 10.3 ± 7.9% with a range of 0-20.4%. Only one setting that produced capsular side effects did not produce internal capsule activation using our model.

3.3.2 Comparison of Dorsal and Ventral Experimental Settings

There were significant differences in the percentage of axons activated between the dorsal and ventral settings in three of the modeled neural pathways (Figure 7). Ansa lenticularis and the GPe→STN pallidosubthalamic tract showed significantly higher activation during dorsal stimulation than ventral stimulation ($p = 0.014$ and $p = 0.011$). The opposite was true for the M1 component of internal capsule, which was significantly more activated with ventral stimulation than dorsal ($p = 0.022$).

There were also noticeable trends in the average recruitment curves created using the dorsal and ventral electrodes (Figure 8). In the ansa lenticularis, the recruitment curves showed a trend towards greater levels of axonal activation with the dorsal electrodes compared to the ventral electrodes as the stimulation amplitude increased. The opposite scenario was true for the internal capsule – ventral electrode stimulation was predicted to cause higher axonal activation than dorsal as the amplitude increased. Similar trends were not present in the recruitment curves for the lenticular fasciculus or pallidosubthalamic tracts.

Table 6. Capsular side effects reported during monopolar review. Monopolar review documents from each participant were screened for capsular side effects including dystonic limb posture, facial muscle contraction, conjugate eye deviation, and dysarthria. The DBS setting parameters that elicited capsular side effects during monopolar review were simulated using the patient-specific computational model and the percentage of internal capsule (IC) axons activated was measured. The DBS settings are indicated as follows: the anode is indicated as a number followed by a $^-$ (e.g. 3^-, indicating that contact 3 is set as the anode). The cathode is indicated with a $^+$ sign. In instances where the case (implanted pulse generator) is set as the cathode, this is abbreviated with a C (e.g. C^+). For settings involving segmented electrode contacts, the active segments are indicated in parentheses following the contact number. Below the active contact information, the amplitude, frequency, and pulse width are listed.

Subject	Side	Setting	Reported side effect	IC activation (%)
UD1001	Right	1^-C^+ 4.5V 130Hz 90us	Dysarthria	4.2
	Left	1^-C^+ 6.5V 130Hz 60us	Dysarthria	2.4
UD1002	Right	2^-C^+ 7V 130Hz 60us	Dysarthria	5.6
	Left	2^-C^+ 6V 130Hz 60us	Dysarthria	0
UD1005	Right	N/A	No capsular effects reported	N/A
UD1013	Left	1^-C^+ 8V 130Hz 60us	Right lower lip and chin twitching and muscle pulling	20.4
UD1015	Right	N/A	No capsular effects reported	N/A
	Left	N/A	No capsular effects reported	N/A
UD1018	Right	$2(abc)^-C^+$ 5V 130Hz 60us	Left lower eyelid twitching and left jaw tightness	5.8
UD1022	Right	1^-C^+ 3V 130Hz 90us	Facial pulling and dysarthria	14
	Left	N/A	No capsular effects reported	N/A
UD1032	Right	N/A	No capsular effects reported	N/A
	Left	2^-C^+ 2.5V 130Hz 90us	Felt tightness in jaw, some pulling of jaw	10.2
UD1034	Right	1^-C^+ 4V 130Hz 60us	Persistent mouth pulling	19.8
	Left	0^-C^+ 3.5V 130Hz 60us	Mouth pulling	20.4

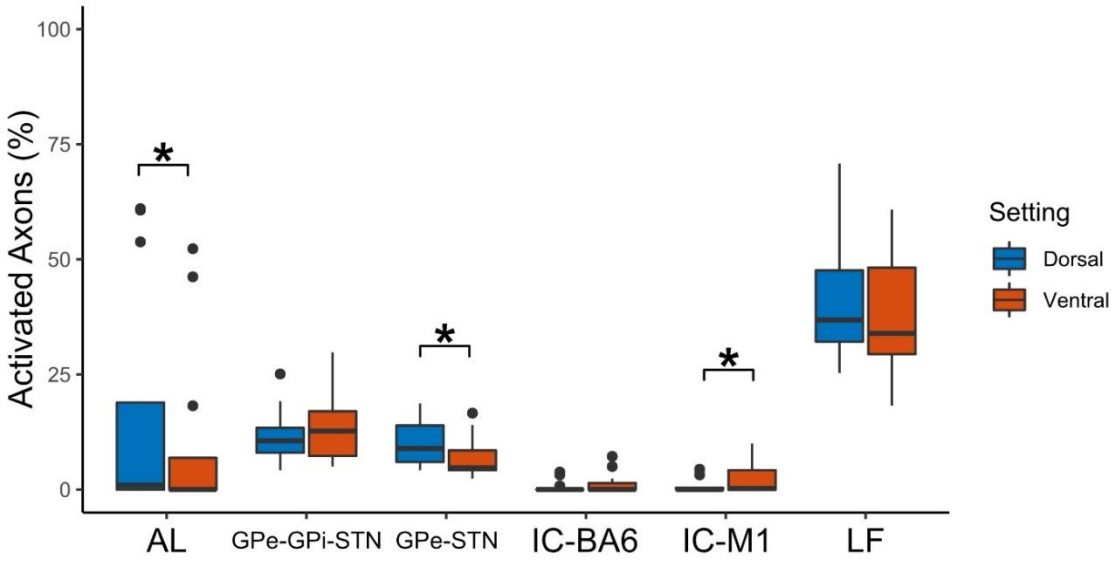

Figure 7. Comparison of activated axons between dorsal and ventral stimulation settings. There were significant differences in the percentage of axons activated in the following pathways: Ansa lenticularis and the GPe→STN pallidosubthalamic tract showed significantly higher activation during dorsal stimulation than ventral stimulation ($p = 0.014$ and $p = 0.011$). The M1 component of internal capsule was significantly more activated with ventral stimulation than dorsal ($p = 0.022$). Paired Wilcoxon Signed Rank tests were used to test for differences in the percentage of axons activated by each setting.

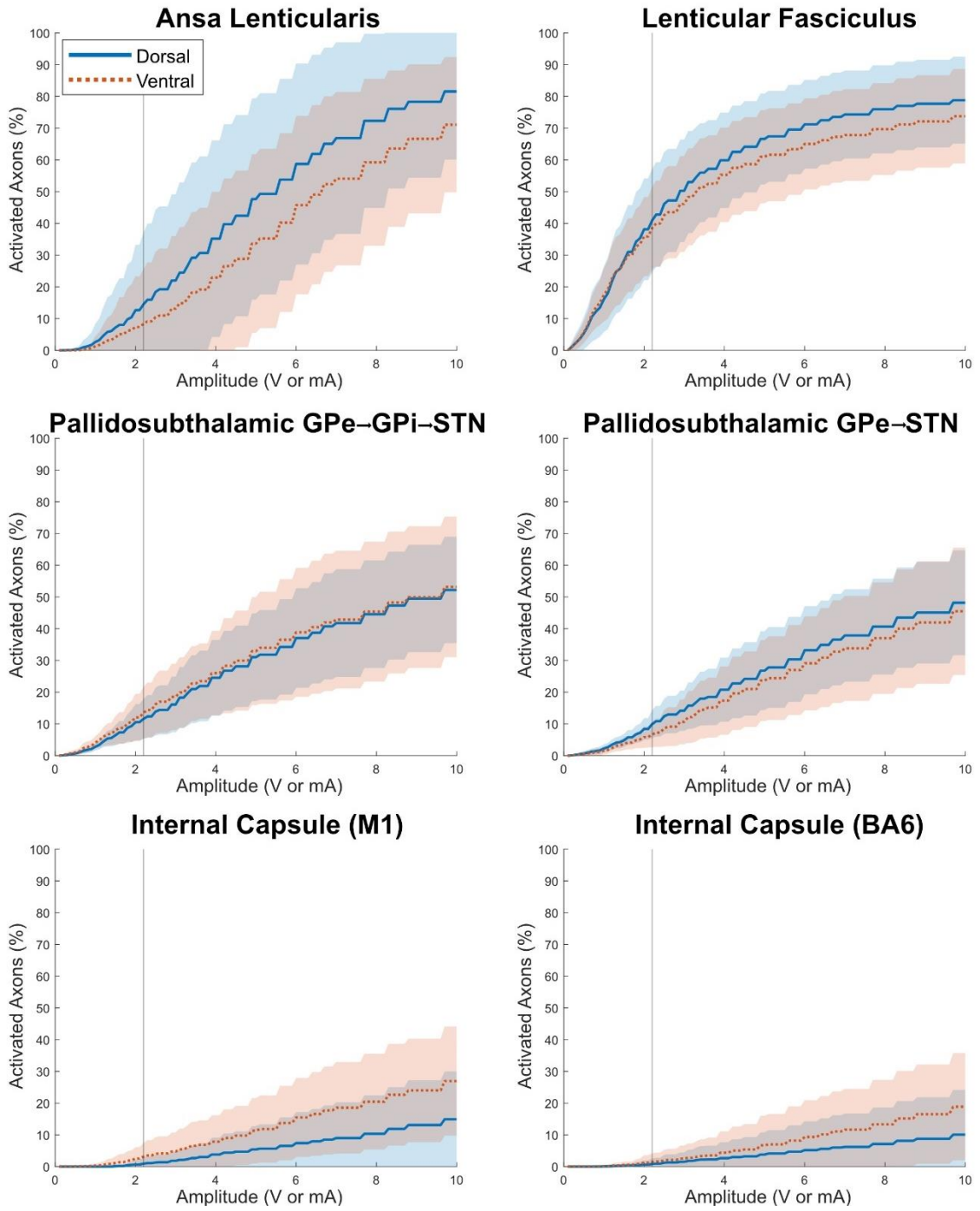

Figure 8. Average recruitment curves for experimental dorsal and ventral setting electrodes. Recruitment curves for each pathway were created by averaging the percentage of activated axons for each participant at 0.1 V/mA amplitude steps between 0 and 10 V/mA . Recruitment curves were created using the electrodes selected for the ventral and dorsal experimental deep brain stimulation settings. The dorsal electrode results are shown in solid blue and the ventral electrode is show in dotted orange. Standard deviations are shown as shaded regions in blue (dorsal) or orange (ventral). The average amplitude selected for the experimental settings (2.23 V/mA) is indicated with a grey vertical line.

3.4 Discussion

The results of this study demonstrate that patient-specific models of the pallidum and nearby fiber tracts can be used to predict the pathways activated by GP-DBS with the methodology described. While opportunities to validate our model in vivo were limited, the predicted activation of the internal capsule for settings eliciting capsular side effects fell within the expected range (Chaturvedi et al., 2010), suggesting that this modeling approach provides reasonable prediction of axonal activation. Using this model, comparisons of pathway activation between experimental dorsal and ventral stimulation settings revealed significant differences in activation of the ansa lenticularis, GPe→STN pallidosubthalamic tract, and internal capsule. Dorsal stimulation led to significantly higher activation in ansa lenticularis and GPe→STN compared to ventral stimulation, while IC activation was greater with ventral stimulation.

We hypothesized that dorsal stimulation would preferentially activate GPe projections to GPi and STN, while ventral stimulation would elicit greater activation in pallidothalamic projections. Our findings only supported one of these hypotheses – dorsal stimulation elicited significantly greater activation of GPe→STN axons than ventral stimulation. These efferent axons are γ-aminobutyric acid (GABA)ergic and provide strong inhibition to the STN, thus potentially driving an overall pro-kinetic effect on the motor system that explains the reports of increased dyskinesia during dorsal GPi stimulation (P. Krack et al., 1998; Vitek et al., 2004; Yelnik et al., 2000). Activation of GPe efferents in a non-human primate model of GP-DBS has been correlated with decreased bradykinesia, even in the absence of GPi efferent activation (M. D. Johnson et al., 2012), suggesting that these fibers may be a viable target for treating bradykinesia. The exact mechanisms by which GPe→STN efferent stimulation elicit a pro-kinetic effect are unclear, but may be related to both direct inhibition of the STN as well as antidromic stimulation of GPe neurons. The GPe is unique in the basal ganglia due to its widespread projections to all other basal ganglia nuclei, allowing it to have powerful influence over the processing of motor information (Hegeman, Hong, Hernández, & Chan, 2016). Antidromic stimulation of GPe through GPe→STN efferents could lead to downstream inhibition of GPi, the primary output nucleus of the basal ganglia, as well as the dorsal striatum. Despite the lack of understanding regarding the precise mechanisms,

using dorsal GP-DBS to activate the GPe→STN pathway may be valuable for patients struggling with severe akinesia or bradykinesia, with the caveat that excessive stimulation may lead to unwanted side effects such as dyskinesias.

The ansa lenticularis was also significantly more activated by dorsal stimulation than ventral stimulation, contrasting our initial hypothesis that ventral stimulation would preferentially activate pallidothalamic tracts. During surgery, DBS electrodes are typically inserted at an angle of 60 degrees from the anterior commissure to posterior commissure line such that the bottom contact of the lead is slightly posterior to the top of the lead (Starr, 2002). Thus, it is not surprising that the dorsal electrode, which would sit more anterior (closer to the initiation points of the AL axons) would cause greater activation of the AL compared to the more posterior ventral electrode due to our choice to restrict the initiation points of AL fibers to the anterior 1/3 of the GPi based on histological findings in the non-human primate (Baron et al., 2001). This topography differs from the anatomical understanding that drove earlier hypotheses about AL activation, however, this scheme of pallidothalamic tract organization, such that pallidothalamic fibers exit from the GPi near their anterior/posterior level of origin, has gained credibility due to pallidotomy outcomes that align with this hypothesis. The restriction of AL fibers to the anterior portion of the GPi is also represented in a newly developed basal ganglia axonal pathway atlas, which was developed in collaboration with world expert neuroanatomists (Petersen et al., 2019). However, there is also evidence that the ansa lenticularis and lenticular fasciculus are not as anatomically separated as it was once believed, and a more appropriate interpretation would be to consider them a continuous pallidothalamic pathway (M. Parent & Parent, 2004). From a functional perspective, the pallidothalamic tract is composed of inhibitory GABAergic efferents that inhibit a variety of nuceli within the thalamus, so activation of this pathway would likely exert an anti-kinetic effect on the motor system. Based on the role of pallidothalamic tracts in the basal ganglia-thalamo-cortical circuit, stimulation of this pathway could be useful for suppressing symptoms such as rigidity and dyskinesias, which are characterized by an excess of motor activity.

The internal capsule also showed differences in activation depending upon the location of DBS, with ventral stimulation eliciting greater activation than dorsal

stimulation. Internal capsule includes axons projecting from many areas of cortex, including primary motor cortex, premotor/supplementary motor areas, and other areas of frontal cortex. The internal capsule passes medially to the GPi, with the primary motor component passing along the posterior end of the nucleus and the premotor/supplementary motor area fibers slightly anterior to the primary motor component. Activation of the internal capsule is often undesirable in DBS due to the variety of side effects including speech impairment, muscle contractions, and dystonic limb posture that can result from IC stimulation (Paul Krack et al., 2002; Starr, 2002). However, there may also be benefits of stimulating IC – activation of a small percentage of IC fibers has been shown to correlate with reduced rigidity in non-human primates (M. D. Johnson et al., 2012; Xu et al., 2011). This may be due to antidromic activation of motor cortex, or downstream effects on spinal motoneurons. Understanding that more ventrally located electrodes in GP-DBS are more likely to activate IC is important to consider in patients who are more sensitive to capsular side effects, or in those who want to specifically manage severe rigidity.

This study is the first to investigate the pathways mediating opposite motor effects in the globus pallidus using patient-specific models of the pallidum. While this study is a valuable step in creating patient-specific models of the pallidum and understanding how electrode location can lead to preferential activation of specific pathways, there were limitations that may have impacted the estimates of pathway activation. This model focused on pathways in and near the pallidum that had been implicated in the opposite effects exhibited in previous studies of GP-DBS. However, there are likely additional pathways and structures that are involved in mediating the effects of GP-DBS, such as the pedunculopontine nucleus, striatopallidal, and striatofugal pathways. Future models of pallidal DBS should take these pathways into account to better understand the role they play in DBS outcomes. Another limitation is that this model was agnostic to axonal morphology – axons in all pathways were modeled as single, non-branching fibers without cell bodies. This contrasts histological studies of the basal ganglia, which have shown profuse collateralization of axons throughout the GPe, GPi, and STN (A. Parent et al., 2000). However, the lack of collateral axons likely has a small effect, as previous modeling studies using multi-compartment cable model axons found that including

axonal branches had a limited effect on the percentage of axons activated, due to the fact that most action potentials developed in the larger, myelinated primary axons (M. D. Johnson & McIntyre, 2008). The omission of cell bodies may also have a minimal effect on model efficacy, since DBS is more likely to exert its effects on axons passing near the stimulating electrode than on local cell bodies (McIntyre et al., 2004).

3.5 Conclusions

This study represents an important step in creating patient-specific models of the pallidum in order to understand mechanisms of GP-DBS. With this computational model, pathways were identified that may mediate the opposite motor effects observed in the globus pallidus, including the GPe → STN projections, ansa lenticularis, and the internal capsule. We expected dorsal stimulation to lead to preferential activation of GPe projections to GPi and STN, and ventral stimulation to activate pallidothalamic projections. However, the results indicated that dorsal stimulation leads to preferential activation of GPe → STN axons and ansa lenticularis, while the only pathway preferentially activated by ventral stimulation was the internal capsule. Further model-based investigations of the globus pallidus may reveal additional important pathways that could lead to improved targeting and outcomes for people with Parkinson's disease.

CHAPTER 4 NEURAL PATHWAYS DRIVING RIGIDITY IMPROVEMENT DURING PALLIDAL DEEP BRAIN STIMULATION FOR PARKINSON'S DISEASE

Maria Linn-Evans, Sommer Amundsen Huffmaster, Jae Woo Chung, Matthew Petrucci, Chiahao Lu, Angela Noecker, Tara Palnitkar, Remi Patriat, Cameron McIntyre, Noam Harel, Scott Cooper, Matthew Johnson, Colum MacKinnon

4.1 Introduction

Parkinson's disease (PD) is a neurodegenerative disorder characterized by a set of cardinal motor symptoms including bradykinesia, tremor, rigidity, and gait dysfunction. Rigidity is a common symptom in PD with over 80% of patients exhibiting segmental and/or axial stiffness (Martin et al., 1973; Mutch et al., 1986). While rigidity alone may not be the most debilitating symptom of PD, reduction of rigidity has been associated

with improvements in levodopa-resistant symptoms such as postural stability and gait coordination (Bartolic, Pirtosek, Rozman, & Ribaric, 2005; Winogrodzka, Wagenaar, Booij, & Wolters, 2005). In addition to its clinical importance, rigidity is a crucial symptom for titrating PD treatments. Treatment early in the disease primarily involves dopamine replacement medications, but as symptoms progress and medication side effects worsen, many individuals with PD choose to undergo deep brain stimulation (DBS) surgery. Rigidity is a particularly valuable assay for DBS efficacy because it responds quickly to stimulation (within seconds to minutes), it remains stable over a programming session, and improvements in rigidity are often predictive of improvement in other symptoms like bradykinesia that have longer wash-in periods (minutes to days) (Paul Krack et al., 2002). For this reason, when programming DBS settings, many clinicians rely on the assessment of rigidity to determine optimal settings. However, the mechanisms by which DBS reduces rigidity are currently poorly understood, which limits the ability of clinicians to target this symptom.

Previous studies have investigated the relationship between DBS stimulation location in globus pallidus (GP) and rigidity with differing outcomes. A number of studies have shown that rigidity scores improve regardless of lead location in GP (Vitek et al., 2012; Yelnik et al., 2000), while others suggest that rigidity improves optimally with stimulation in ventral regions of the GPi (P. Krack et al., 1998). Since rigidity results from excessive muscle tone, it is logical to hypothesize that activation of anti-kinetic pathways, such as those thought to be preferentially activated by ventral GP-DBS, would be effective in reducing rigidity. One limitation of these studies is the focus on anatomical location within GP, as opposed to considering activation of specific neural pathways in and around GP. These studies also failed to quantify the extent of current spread for each DBS setting, so it is not clear what regions and pathways were activated. In order to understand the specific pathways involved in mediating rigidity, a small number of studies have implemented computational models of DBS. Modeling studies in non-human primates investigating both subthalamic nucleus (STN) and GP-DBS suggest that DBS settings that activate a small percentage of internal capsule axons may be the most effective in treating rigidity (M. D. Johnson et al., 2012; Xu et al., 2011). Improvements in rigidity with STN-DBS in people with PD have been associated with

activation of tissue volumes near pallidofugal pathways, including ansa lenticularis, lenticular fasciculus, and pallidosubthalamic tracts (Avecillas-Chasin & Honey, 2020). Additionally, STN-DBS locations that are most effective in reducing rigidity have been shown to have significant structural connectivity with SMA and prefrontal cortex regions (Akram et al., 2017).

The relationship between model-based DBS pathway activation and rigidity has not been assessed in people with GP-DBS, making this study an important step towards understanding how GP-DBS can be targeted to optimize treatment of an individual's symptoms. The goals of this study were to characterize the effects of GP-DBS on rigidity and use patient-specific GP-DBS models to identify neural pathways associated with the response of rigidity to DBS. We hypothesized that GP-DBS would significantly improve rigidity and that activation of pathways near ventral GPi, such as the pallidothalamic tracts and internal capsule, would be the most predictive of improvements in rigidity.

4.2 Methods

4.2.1 Participants

Nine individuals (3 women, 6 men, age = 62.8 ± 8.6) being treated with pallidal DBS for Parkinson's disease participated in this study. Inclusion criteria were diagnosis of idiopathic Parkinson's disease by a movement disorders neurologist, existing deep brain stimulation system implanted in globus pallidus, and presence of pre-surgical 7T MRI scans and a post-surgical CT. Exclusion criteria included a history of musculoskeletal disorders affecting movements of the limbs, neurological disorders besides PD, history of dementia or cognitive impairment, or post-operative complications that could affect patient safety or confound experimental results. All participants performed movement tasks after a 24-hour withdrawal period from extended release antiparkinson medications (e.g. Sinemet CR) and a 12-hour withdrawal period from immediate release antiparkinson medications. All study procedures were approved by the University of Minnesota Institutional Review Board and all participants provided written informed consent according to the Declaration of Helsinki.

Table 7. Demographics of study participants. Movement Disorder Society Unified Parkinson's Disease Rating Scale III (MDS-UPDRS III) assessment was performed OFF medication and OFF stimulation. Levodopa daily equivalent (LDE) was determined based on the Tomlinson formula (Tomlinson et al., 2010). DBS = Deep brain stimulation

ID	Sex	Age	Years since diagnosis	MDS-UPDRS III	LDE (mg)	Implant Side	DBS Device
UD1001	M	53	15	56	696	Bilateral	Medtronic Activa
UD1002	M	56	11	43	1010	Bilateral	Medtronic Activa
UD1005	F	82	11	50	825	Right	Abbott Infinity
UD1013	M	71	8	48	950	Left	Medtronic Activa
UD1015	F	63	5	66	800	Bilateral	Abbott Infinity
UD1018	F	60	9	51	1000	Right	Abbott Infinity
UD1022	M	62	11	67	150	Bilateral	Abbott Infinity
UD1032	M	64	9	67	800	Bilateral	Medtronic Activa
UD1034	M	54	5	52	850	Bilateral	Medtronic Activa

4.2.2 Experimental Deep Brain Stimulation Settings

The primary goal of this project was to evaluate the effects of various GP-DBS settings on rigidity, which required the development of experimental DBS settings for each participant prior to the motor task visits. StimVision, a software tool used to estimate the volume of tissue activated by DBS, was used to identify stimulation settings that theoretically biased DBS to either dorsal or ventral aspects of the targeted nucleus (A. M. Noecker et al., 2018). Rigidity was also tested on each participant's clinical DBS setting, which was defined as the setting optimized for therapeutic benefit by the patient's physician.

Prior to DBS surgery, all participants underwent a 7T MRI at the Center for Magnetic Resonance Research at the University of Minnesota using a Siemens console, SC72 gradient coil, and 32-channel head coil. The imaging protocol included high-

resolution anatomical scans (T1 and T2 weighted) as well as diffusion weighted imaging (DWI) using protocols which have been described in previous publications (Abosch et al., 2010; Duchin et al., 2012; Lenglet et al., 2012). One month following surgery, participants underwent a routine clinical CT scan, which was registered with the T1-weighted MRI to allow for lead localization. Manual segmentations of basal ganglia nuclei (GPe, GPi, STN, SN and RN) were extracted from the T2-weighted anatomical images by research staff experienced in this technique (Duchin et al., 2018).

Patient-specific anatomical models of each brain hemisphere for each subject were created based on their 7T MRI data (Gunalan et al., 2017). The manually segmented basal ganglia nuclei were constructed into 3D volumes for visualization with the MRI slice data. The T1-weighted MRI was used as the base image for data co-registration, and the patient anatomical model was merged with the post-operative CT image to identify the DBS electrode location in the brain. The patient-specific imaging data, anatomical volumes, and DBS electrode location were loaded into the StimVision software tool to assist with the definition of model-based DBS settings that would be used in the clinical experiments. Volume of tissue activated (VTA) estimates of stimulation spread were used to guide selection of the contact and amplitude for the experimental DBS setting (Chaturvedi et al., 2013). The pulse width (60 us) and stimulation frequency (130 Hz) were held constant for all DBS settings.

For each brain hemisphere, an expert in DBS modeling blinded to the clinical settings (CCM) used the patient-specific StimVision model to select an electrode contact that most closely fit the anatomical designation of dorsal or ventral placement within the nucleus. Next, VTA estimates were used to define a stimulation amplitude through the selected electrode contact which fulfilled the following criteria: 1) Concentrated stimulation in the targeted anatomical area, 2) Avoided stimulation spillover to the non-targeted anatomical area, and 3) Avoided stimulation spillover to the internal capsule. Definition of the StimVision-derived experimental DBS settings was blinded to any information about the subjects, including the clinically determined settings. The final settings used during this experiment are described in Table 8. The electrodes used for each setting were localized relative to the ventral GPi border using a custom MATLAB script. The distance along the dorsal/ventral axis between the center of the active

electrode and the most ventral point of the GPi was calculated for each individual setting. The distances averaged by setting are presented in Table 9 and histograms showing the electrode distributions relative to the ventral GPi border are presented in Figure 9.

Prior to using the experimental DBS settings during a movement task visit, all participants participated in a screening visit to evaluate the novel settings for potential side effects. The screening visit was conducting in the morning after overnight withdrawal from anti-parkinsonian medications, or after 24-hour withdrawal from extended/controlled release anti-parkinsonian medications. The StimVision-derived dorsal and ventral DBS settings were programmed and individually tested by a movement disorders neurologist or nurse practitioner with experience programming and testing DBS settings. Each setting remained ON for a sufficient duration of time (~1 hour) to evaluate for side effects. The goal of the screening visit was to assess the tolerance of the participant to the dorsal and ventral settings in order to reduce the likelihood of an adverse event during future data collection visits. All settings presented in this study were tolerated by the participants during both the screening visit and data collection.

Table 8. Tested deep brain stimulation settings. The active contacts are listed under the Clinical, Dorsal and Ventral Settings columns. The anode is indicated as a number followed by a $^-$ (e.g. 3^-, indicating that contact 3 is set as the anode). The cathode is indicated with a $^+$ sign. In instances where the case (implanted pulse generator) is set as the cathode, this is abbreviated with a C (e.g. C^+). For settings involving segmented electrode contacts, the active segments are indicated in parentheses following the contact number. After the contact information, the amplitude, frequency, and pulse width are listed.

Subject ID	Lead	Implant Side	Clinical Settings	Dorsal Settings	Ventral Settings
UD1001	Medtronic 3389	Left	$1^-2^-C^+$, 5V, 130Hz, 60us	3^-C^+, 3V, 120Hz, 60us	1^-C^+, 3V, 120Hz, 60us
	Medtronic 3387	Right	$1^-2^-C^+$, 4.5V, 125Hz, 60us	3^-C^+, 3V, 120Hz, 60us	1^-C^+, 3V, 120Hz, 60us
UD1002	Medtronic 3389	Left	2^-C^+, 3.6V, 180Hz, 60us	3^-C^+, 2V, 120Hz, 60us	2^-C^+, 2V, 120Hz, 60us
		Right	2^-C^+, 3.5V, 180Hz, 60us	3^-C^+, 2V, 120Hz, 60us	2^-C^+, 2V, 120Hz, 60us
UD1005	Abbott 6172	Right	2(abc)$^-C^+$, 4mA, 130Hz, 90us	4^-C^+, 3mA, 120Hz, 60us	2(bc)$^-C^+$, 3mA, 120Hz, 60us
UD1013	Medtronic 3389	Left	2^-C^+, 3.5V, 130Hz, 60us	2^-C^+, 2V, 120Hz, 60us	1^-C^+, 2V, 120Hz, 60us
UD1015	Abbott 6172	Left	3(c)$^-C^+$, 3mA, 200Hz, 90us	4^-C^+, 2mA, 120Hz, 60us*	2(c)$^-C^+$, 1mA, 120Hz, 60us
		Right	3(abc)$^-C^+$, 4mA, 200Hz, 90us	4^-C^+, 2mA, 120Hz, 60us*	2(b)$^-C^+$, 1mA, 120Hz, 60us
UD1018	Abbott 6172	Right	2(abc)$^-C^+$, 3.8mA, 130Hz, 60us	4^-C^+, 2.5mA, 120Hz, 60us	2(ab)$^-C^+$, 2.5mA, 120Hz, 60us
UD1022	Abbott 6172	Left	3(abc)$^-C^+$, 3.7mA, 130Hz, 90us	3(b)$^-C^+$, 2mA, 120Hz, 60us	2(b)$^-C^+$, 2mA, 120Hz, 60us
		Right	2(abc)$^-C^+$, 3.7mA, 130Hz, 90us	3(a)$^-C^+$, 2mA, 120Hz, 60us	2(a)$^-C^+$, 2mA, 120Hz, 60us
UD1032	Medtronic 3389	Left	2^-3^+, 3.7V, 130Hz, 90us	3^-C^+, 2V, 120Hz, 60us	2^-C^+, 2V, 120Hz, 60us
		Right	1^-2^+, 2.7V, 130Hz, 90us	3^-C^+, 2V, 120Hz, 60us	1^-C^+, 2V, 120Hz, 60us
UD1034	Medtronic 3389	Left	2^-C^+, 3.4V, 130Hz, 60us	2^-C^+, 2V, 120Hz, 60us	0^-C^+, 2V, 120Hz, 60us
		Right	1^-C^+, 2.8V, 130Hz, 60us	3^-C^+, 2V, 120Hz, 60us	1^-C^+, 2V, 120Hz, 60us

Table 9. Average electrode locations. Average distances between the ventral globus pallidus internus (GPi) border and the active electrode were calculated for the electrodes used in each deep brain stimulation setting. Distance was measured along the dorsal/ventral axis from the most ventral point of the GPi to the center of the active electrode. Higher values indicate that the electrode is located more dorsally in the nuclei.

Setting	Mean distance ± SD (mm)
Clinical	4.9 ± 1.4
Ventral	3.9 ± 1.3
Dorsal	6.5 ±1.5

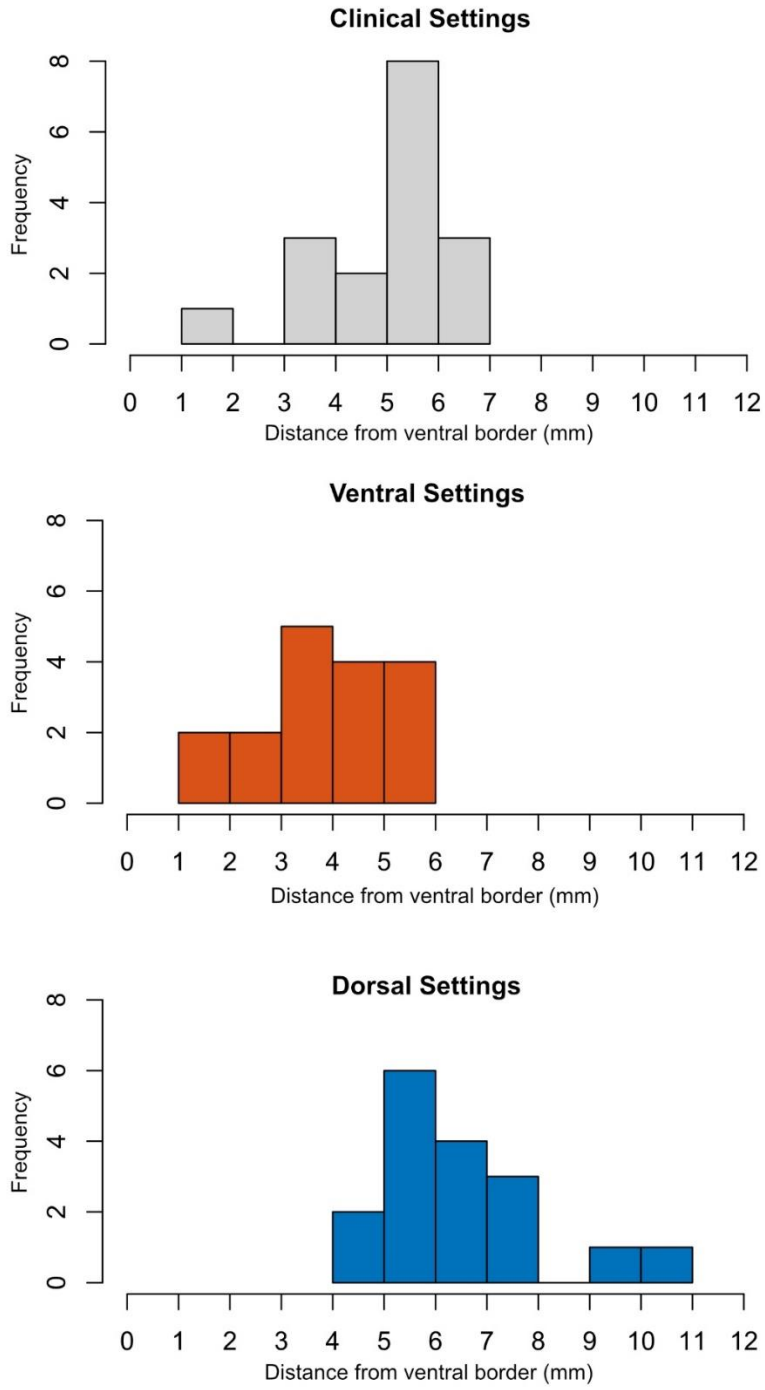

Figure 9. Distribution of electrode locations. Distances between the ventral globus pallidus internus (GPi) border and the active electrode for each deep brain stimulation setting were calculated along the dorsal/ventral axis. The distribution of electrode locations for each setting is presented as a histogram, with the distance in mm along the x-axis and the number of electrodes along the y-axis.

4.2.3 Rigidity Data Collection and Analysis

Participants completed a separate data collection visit for each tested DBS setting (OFF, Clinical, Dorsal, Ventral). Visits were separated by at least 1 week. DBS settings used on the day of data collection were set by a movement disorders neurologist not involved in data collection to ensure that participants and study staff were blinded to the setting. All testing occurred after a one-hour DBS wash-in period. All participants underwent an assessment of motor symptom severity using the Movement Disorder Society Unified Parkinson's Disease Rating Scale (MDS-UPDRS) Part III evaluation. This data, as well as demographic data, were stored and managed using REDCap electronic data capture tools (Harris et al., 2009). Angular impulse, a quantitative measure of forearm rigidity calculated from an integrated torque signal, was obtained used a custom-built robotic manipulandum (Linn-Evans et al., 2020). Trials were collected on the right and left sides in subjects with bilateral leads, or on the side contralateral to the lead in subjects with unilateral DBS. Trials were also collected with or without an activation maneuver (tapping the contralateral hand on the leg), a technique that is used clinically to elicit or enhance rigidity. Each trial was 45 seconds long. Calculation of rigidity measures was performed using custom MATLAB software (MathWorks, Natick, MA, USA).

4.2.4 Patient-Specific Axon Modeling

Patient-specific models of the major axonal pathways within and near the globus pallidus, as described in Chapter 3, were used to estimate the percentage of axons activated in each pathway for the tested DBS settings. Individual 7T MRI data was used to segment basal ganglia nuclei and run probabilistic tractography to identify the location of white matter tracts. Multi-compartment cable models of axons were populated throughout the nuclei and tracts. A finite element model analysis was performed in order to estimate the extracellular voltages throughout the area of interest, which were then interpolated across the axonal compartments. Simulations were run in NEURON to evaluate the percentage of axons in each pathway activated during DBS. The computational model included six neural pathways: ansa lenticularis (AL), lenticular

fasciculus (LF), two pallidosubthamic tracts (GPe → GPi → STN and GPe → STN), and internal capsule projecting from motor cortex (IC-M1) and Brodmann's area 6 (IC-BA6).

4.2.5 Statistical Analyses

R statistical software was used to perform all analyses (R Core Team, 2021). Rigidity scores were compared between the OFF stimulation condition and each DBS setting using paired Wilcoxon signed-rank tests.

In order to evaluate the relationship between individual pathway activation and rigidity severity, correlations were computed between the percentage of activated axons in each pathway and the change in the quantitative rigidity score. Kendall's rank correlation coefficients were calculated due to Shapiro-Wilk tests showing a non-normal distribution. P-values were corrected for multiple comparisons using the Bonferroni method. A negative change in rigidity score indicated a decrease in rigidity.

Linear mixed-effect (LME) models were generated using the lme4 package (Bates, Mächler, Bolker, & Walker, 2015) to analyze the relationship between changes in rigidity score and the activation of multiple pathways. In order to adjust for the right skewed distribution of the percentage of activated axons (a large number of settings led to little or no activation), the percentage data were log transformed. The transformation was performed using $\ln(x + 1)$ to ensure zeros in the raw dataset would have a real solution. The LME model was generated with a dataset derived from 15 GP-DBS sides, consisting of 45 different pathway activation profiles and 90 rigidity tests scores. Change in rigidity score relative to the OFF DBS state was set as the dependent variable and the percentage of activated axons (log transformed) in each pathway were set as fixed-effects. The LME model included subject as a random intercept to account for variability between individuals. Kenward-Roger approximation was used to calculate p-values for the fixed-effects. Conditional and marginal R^2 values were calculated for each linear mixed-effect model.

The LME models were also used to create a dataset of predicted change in rigidity scores based on the percentage of activated axons in each pathway. These model-predicted values were compared to the actual measured values for each subject and a

Kendall's rank correlation was computed to evaluate the predictive value of each model. The significance level for all tests was set at $\alpha = 0.05$

4.3 Results

4.3.1 Effect of GP-DBS on Rigidity

Rigidity scores with and without an activation maneuver showed a significant difference between OFF stimulation and on clinical DBS settings ($p < 0.0001$). There were no significant differences in rigidity scores measured OFF stimulation and on the experimental dorsal or ventral DBS settings (Figure 10).

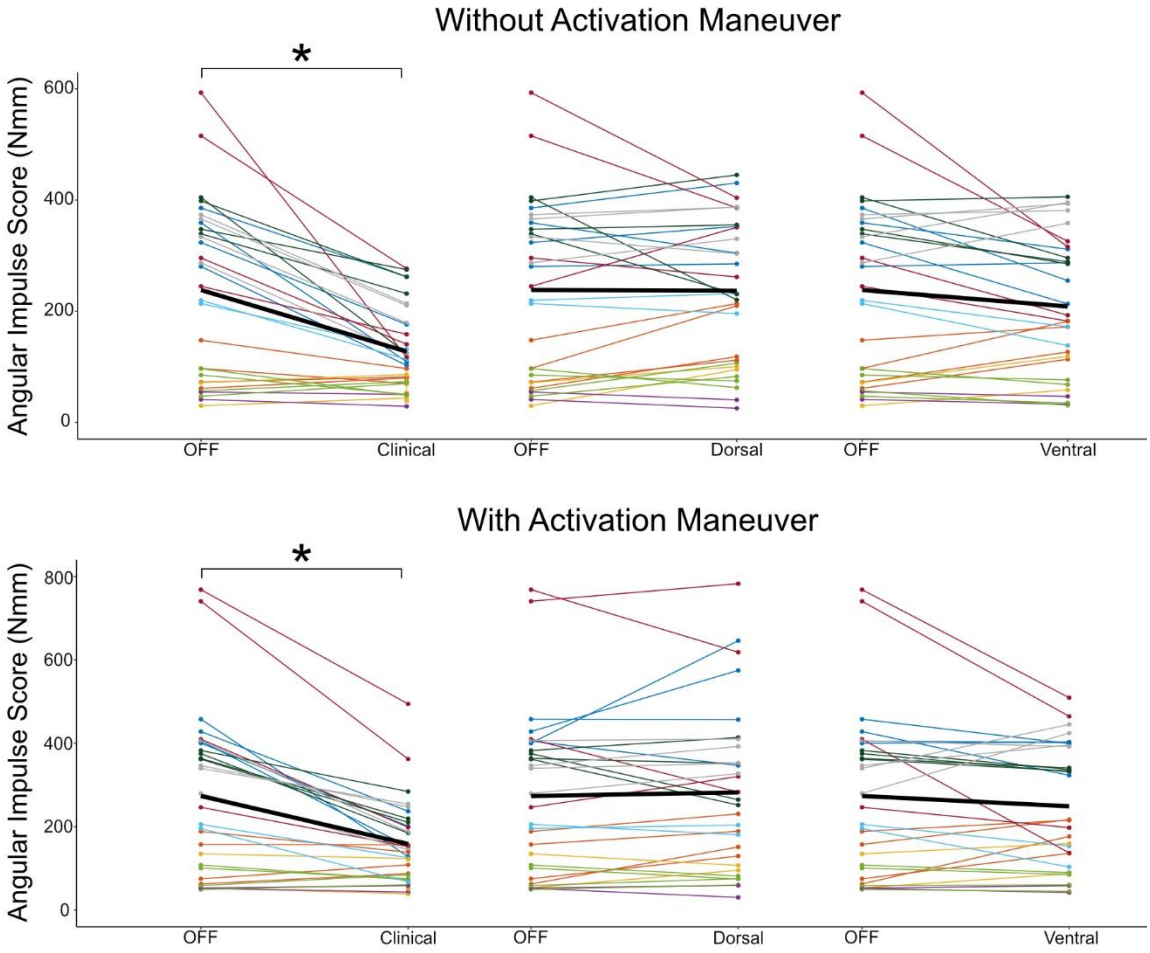

Figure 10. Change in rigidity scores between OFF stimulation and tested DBS settings. The thick black line indicates the average change in rigidity scores between OFF and the tested setting, while thin colored lines represent the change in rigidity scores for individual participants. Rigidity scores were compared between the OFF condition and each DBS setting using paired Wilcoxon signed-rank tests. *=p<0.0001.

4.3.2 Correlation Between Pathway Activation and Rigidity

There were significant correlations identified between the change in rigidity and the percentage of axons activated in the modeled pathways. Correlation coefficients and p-values are shown in Table 10. For angular impulse scores without an activation maneuver, improvement in rigidity correlated with increased activation in internal capsule and GPe→GPi→STN. With the addition of the activation maneuver, improvement in angular impulse scores showed significant correlations with activation of all pathways except lenticular fasciculus.

Table 10. Correlation results. Kendall's rank correlation coefficients were calculated to evaluate the relationship between the percentage of axons activated in each pathway and the change in angular impulse (rigidity) scores. P-values were adjusted for multiple comparisons with a Bonferroni correction. BA6 = Brodmann's area 6, M1 = primary motor cortex.

	Angular Impulse without an Activation Maneuver		Angular Impulse with Activation Maneuver	
Pathway	Kendall's Tau	p-value	Kendall's Tau	p-value
Ansa lenticularis	-0.12	0.60	-0.20	0.047*
Lenticular fasciculus	-0.16	0.15	-0.15	0.24
Pallidosubthalamic (GPe→GPi→STN)	-0.21	0.018*	-0.23	0.009*
Pallidosubthalamic (GPe → STN)	-0.13	0.47	-0.19	0.038*
Internal capsule (BA6)	-0.40	<0.001*	-0.35	<0.001*
Internal capsule (M1)	-0.30	<0.001*	-0.28	0.001*

4.3.3 Linear-Mixed Effect Models

Linear mixed-effect models were used to identify pathways that best predicted improvement in quantitative rigidity scores. A detailed summary of the LME models is included in Table 11. Marginal R^2 values (representing the variance explained by the fixed-effects alone) were 0.41 for rigidity without an activation maneuver and 0.36 for rigidity with an activation maneuver. The conditional R^2 values (representing the

variance explained by the entire model, including random effects) were slightly larger at 0.53 and 0.44 for the models without and with an activation maneuver, respectively. Both LME models showed a significant effect of the BA6 component of internal capsule. The location of this significant pathway relative to the globus pallidus and an example lead is shown in Figure 11.

Table 11. Linear mixed-effect model results. Coefficients (B), p-values, and R^2 values resulting from the linear mixed-effect model. Kenward-Roger approximation was used to calculate p-values for the fixed-effects. SE = standard error, AL= ansa lenticularis, LF = lenticular fasciculus, IC-BA6 = internal capsule from Brodmann's area 6, IC-M1 = internal capsule from primary motor cortex.

Without an Activation Maneuver			**With an Activation Maneuver**		
Model	B (SE)	p-value		B (SE)	p-value
Intercept	182 (88)		Intercept	95 (102)	
AL	-0.34 (8.5)	0.97	AL	-16 (9.9)	0.13
LF	-36 (24)	0.17	LF	-20 (27)	0.50
GPe-GPi-STN	-29 (22)	0.20	GPe-GPi-STN	8.2 (25)	0.76
GPe-STN	10 (20)	0.62	GPe-STN	-4.3 (23)	0.86
IC-BA6	-84 (17)	<0.001*	IC-BA6	-71 (19)	0.001*
IC-M1	-3.9 (13)	0.78	IC-M1	-19 (15)	0.24
R^2 (marginal/conditional)	0.41/0.53		R^2 (marginal/conditional)	0.36/0.44	

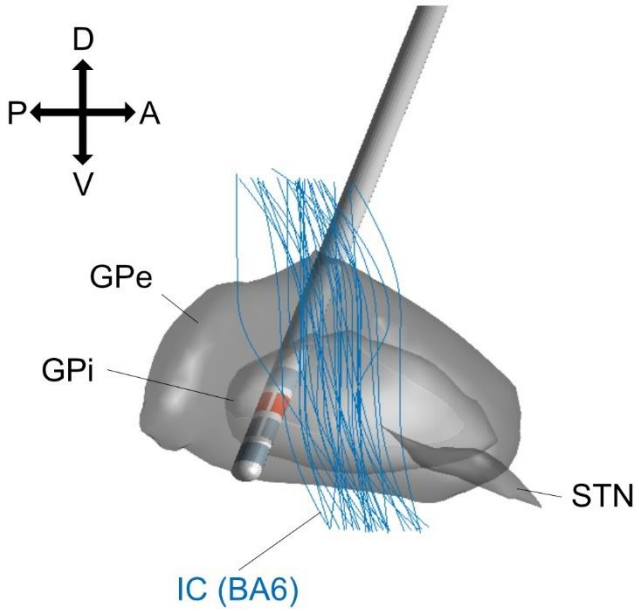

Figure 11. Pathways identified as significant predictors of rigidity improvement. This image shows the fibers in internal capsule from Brodmann's area 6 activated by stimulation by an electrode in globus pallidus internus. The active electrodes are show in red. Activation of this pathway was identified in the linear-mixed effect model as a significant predictor of rigidity improvement during pallidal deep brain stimulation.

4.3.4 Model-based Predictions

There were significant correlations between the model-predicted percent change in rigidity and the measured change in rigidity for both testing conditions (with and without and activation maneuver) as indicated by the results of the Kendall's rank correlation (Figure 12).

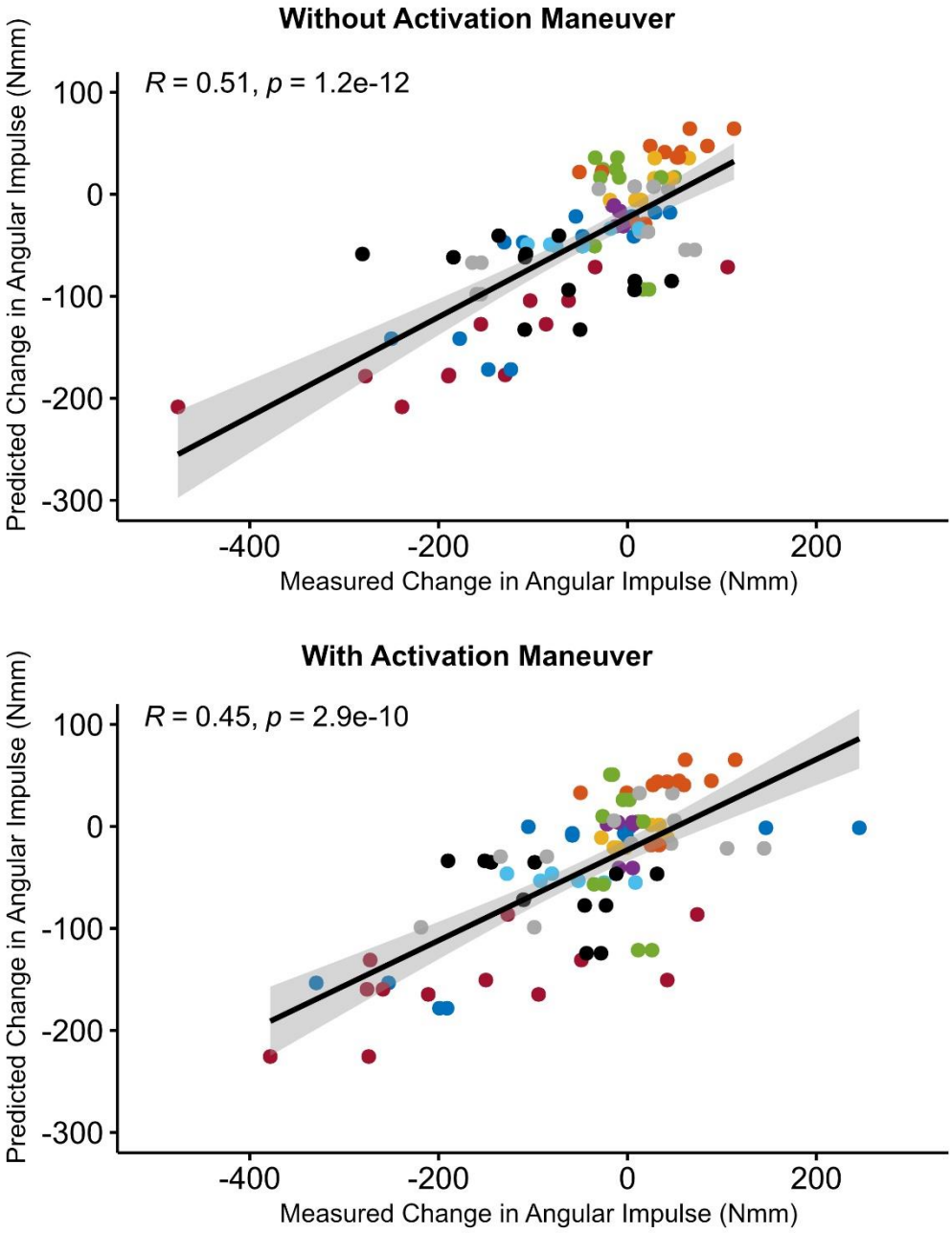

Figure 12. Model predicted change in rigidity score compared to measured change in rigidity score. Pathway activation values were fed into the linear-mixed effect model to create a dataset of predicted change in rigidity scores. The relationship between the measured change in rigidity scores and the linear-mixed effect model predicted scores was assessed with a Kendall's rank correlation coefficient. Points represent individual change scores, with each color assigned to a unique individual. The regression line is shown in black with the 95% confidence interval indicated by the grey shading.

4.4 Discussion

The goal of this study was to identify neural pathways activated by GP-DBS associated with improvements in rigidity. The results of the linear mixed-effect models suggest that there are specific pathways that are better predictors of rigidity improvement. The LME models for both rigidity score conditions (with and without an activation maneuver) found a significant effect of internal capsule activation, specifically fibers projecting from Brodmann's area 6. The results of the individual correlation analyses between pathway activation levels and improvement in rigidity scores indicated that higher levels of activation of GPe→GPi→STN and IC pathways were correlated with reduced rigidity without an activation maneuver, while increased activation of all pathways except the lenticular fasciculus were significantly correlated with rigidity scores with an activation maneuver.

The involvement of the internal capsule in predicting rigidity improvement has been previously reported in non-human primates (M. D. Johnson et al., 2012). This study found that activation of a small percentage of IC fibers (<10%) during DBS correlated with the best improvements in rigidity. Human studies have also reported greater rigidity improvement with stimulation in the ventral GP (P. Krack et al., 1998), which based on our findings in Chapter 3 is more likely to involve greater internal capsule activation than dorsal settings. Involvement of the IC in rigidity suppression ties in well to the hypotheses that parkinsonian rigidity is mediated by abnormalities in the transcortical long-latency stretch reflex (Tatton & Lee, 1975) or dysfunction of spinal pathways mediating group Ia reciprocal inhibition and group Ib autogenetic inhibition (Delwaide, 2001; Delwaide et al., 1991). In particular, the long-latency stretch reflex is reported to be exaggerated in individuals with PD and extensive rigidity (Tatton & Lee, 1975). Activation of the internal capsule with DBS could lead to antidromic activation of motor cortex that modulates firing patterns and excitability at the cortical level, or it could send orthodromic signals via descending pathways to exert influences on spinal motor neuron and interneuron excitability. Interestingly, our model suggests that improvement in rigidity is predicted most strongly by activation of internal capsule fibers projecting from Brodmann's area 6, which contains premotor and supplementary motor areas, as opposed to those projecting from primary motor cortex. The supplementary motor area (SMA) is a

region located anteromedial to primary motor cortex that has been implicated in a wide variety of complex motor behaviors, many of which seem related to parkinsonian rigidity. Early lesion studies in non-human primates found that damage to the SMA led to hypertonia, spasticity, and resistance to passive movement in the flexor muscles, as well as changes in posture and grasp reflexes (Travis, 1955). Stimulation of the SMA in non-human primates also modulated the response of M1 neurons to a passive movement, primarily leading to inhibition of the M1 neurons (Hummelsheim, Wiesendanger, & Bianchetti, 1986). The SMA has been shown to have abnormally decreased activity in individuals with Parkinson's disease, particularly in the rostral regions (Sabatini et al., 2000), which could lead to abnormal modulation of the long-latency stretch reflex (Colum D. MacKinnon et al., 2000). A case study in a man with an infarction of the right SMA found that the injury led to increased long-latency stretch reflexes and increased muscle tone at the wrist (Dick et al., 1987), so it seems possible that decreased SMA activity in PD could lead to disinhibition of M1, an exaggerated long-latency stretch reflex, and thus increased rigidity. Numerous studies have also investigated using SMA as a target for neuromodulation in PD. Excitatory repetitive transcranial magnetic stimulation of SMA has been associated with modest improvements in clinical ratings of PD severity (Hamada et al., 2008). Additionally, STN DBS locations that are most effective in reducing rigidity have been shown to have significant structural connectivity with SMA and prefrontal cortex regions (Akram et al., 2017). Our results suggest that DBS activating internal capsule axons projecting from SMA/premotor cortex is associated with improvements in rigidity, possibly due to neuromodulatory effects counteracting the underactivation of SMA in individuals with PD. Decreased activation in SMA may lead to decreased modulation of the long-latency reflex, a transcortical reflex that has been implicated in rigidity. Alternatively, activation of IC fibers may also normalize dysfunctional spinal pathways that contribute to increased muscle tone and stretch-evoked activity in PD including Ib interneuron activity, which has been implicated in the shortening reaction, an abnormal contractile response evoked in a shortened muscle while an antagonist muscle is stretched (Ruiping Xia et al., 2009). While the role of SMA in PD has been explored in numerous studies, little is known

about the role of premotor cortex in mediating PD pathology, and it is unclear if activation of this region may also play a role in reducing rigidity.

The LME indicated that activation of the IC-BA6 by DBS was the best predictor of rigidity improvements, but the correlation analyses showed that activation of additional pathways was also correlated with improvements in rigidity. While these pathways may not be the primary driver of rigidity improvements, they may still contribute to the overall response. For example, activation of IC-M1 axons could also lead to changes in the long-latency stretch reflex via antidromic activation of motor cortex. Activation of pallidosubthalamic pathways likely exerts widespread modulatory effects on the basal ganglia due to the GPe having projections to all the major basal ganglia nuclei. While the effect on rigidity is less clear in this scenario, reductions in abnormal oscillatory activity throughout the basal ganglia could lead to improvements in a variety of symptoms.

While our LME model did explain nearly 50% of variance in rigidity scores, the R^2 values indicate that there are sources of variability that are not captured by our current model. It is possible that there are additional neural pathways activated by GP-DBS that mediate rigidity that were not included in our computational model, such as striatofugal or striatopallidal pathways. Another limitation was the heterogeneity of the PD phenotypes represented in this sample. While some individuals showed meaningful improvements in rigidity with GP-DBS, others had minimal rigidity that was relatively unaffected by stimulation. It is possible that PD subtypes have abnormalities in different pathways and structures such that DBS settings that work well for reducing rigidity in one phenotype (e.g. akinetic-rigid) may not be effective for another phenotype (e.g. tremor dominant).

4.5 Conclusions

The results of this study indicate that internal capsule activation by GP-DBS plays an important role in reducing parkinsonian rigidity. In particular, profound decreases in rigidity were associated with activation of internal capsule fibers projecting from Brodmann's area 6, which contains premotor cortex and supplementary motor area. Stimulation of the internal capsule may modulate rigidity severity via antidromic activation of supplementary motor area, leading to a reduced long-latency reflex response, or by modulating input to spinal motoneurons. The identification of this

pathway as a potential DBS target for the reduction of rigidity is a major step towards symptom-specific individualization of GP-DBS.

CHAPTER 5 CONCLUSIONS AND FUTURE DIRECTIONS

5.1 Summary of Findings

The primary goal of this dissertation was to address heterogeneity in both the presentation of parkinsonian rigidity and the response of rigidity to deep brain stimulation. Chapter 2 described an investigation into the effects of REM sleep without atonia on the presentation of rigidity in population of individuals with mild-to-moderate PD. Chapter 3 described the development of a patient-specific computational model of pallidal DBS and identified pathways that were preferentially activated between dorsal and ventral stimulation locations. Finally, the same pallidal DBS model was used in Chapter 4 to determine which neural pathways led to optimal reduction in rigidity.

The findings from Chapter 2 indicates that people with PD and RSWA have dysfunction in the regulation of muscle tone during both sleep and wakefulness. This finding also suggests that the presence of RSWA alongside PD may predict greater brain stem neuropathology. While previous studies have found increased symptom severity in individuals with PD and idiopathic REM sleep behavior disorder, our study shows that in mild to moderate PD, the presence of RSWA (even without a diagnosis of idiopathic RBD) is associated with increased rigidity magnitude and symmetry. The mechanism underlying this elevated rigidity magnitude and symmetry is unclear, but may be due to either increased disease severity or increased involvement of subcortical pathways.

The work presented in Chapter 3 outlines an important step in creating patient-specific models of the pallidum in order to understand mechanisms of GP-DBS. Pathways were identified with this model that may mediate the opposite motor effects observed in the globus pallidus between the dorsal and ventral regions. The results of this study indicate that dorsal stimulation may lead to preferential activation of GPe → STN axons and ansa lenticularis, while ventral stimulation may preferentially activate internal capsule. These findings provide increased understanding of pallidal deep brain

stimulation and the mechanisms underlying the reported pro-kinetic effects of dorsal stimulation and anti-kinetic effects of ventral stimulation.

Finally, the results of Chapter 4 show that internal capsule activation by GP-DBS plays an important role in reducing parkinsonian rigidity. Specifically, decreases in rigidity were associated with activation of fibers projecting from Brodmann's area 6, which contains premotor cortex and supplementary motor area. Stimulation of the internal capsule may modulate rigidity severity via antidromic activation of supplementary motor area, leading to a reduced long-latency reflex response, or by modulating input to spinal motoneurons. Identifying DBS targets for the reduction of rigidity using a patient-specific model of GP-DBS is a major step towards symptom-specific individualization of GP-DBS, while also suggesting possible mechanisms underlying parkinsonian rigidity.

5.2 Future Directions

The results of these studies show that there is value in investigating potential sources of heterogeneity in the presentation of Parkinson's disease symptoms as well as in the individual responses to therapies including deep brain stimulation. Regarding RSWA, an important next step is to investigate the relationship between this symptom and the rate of disease progression. We found that individuals with PD and RSWA had greater rigidity severity and symmetry compared to similar people with PD and no RWSA, which suggests that the rate of disease progression may be increased in this population. Future work should also look into other signs that may be associated with variable disease presentation in PD. Being able to predict symptom presentation and progression based on other measurable signs has great clinical value – it can help clinicians counsel patients with more specificity and may also influence treatment decisions in order to make them as targeted as possible.

Deep brain stimulation is a therapy for PD that has the potential to provide symptom-specific treatment by targeting structures associated with individual symptoms. Using computational models of neural structures is a valuable tool for identifying the unique pathways that may be associated with certain symptoms in PD. Future models of the human globus pallidus may benefit from modeling additional pathway in and around

the pallidum (e.g. including striato-pallidal pathways) and including morphological features like the axonal branching that has been described throughout the basal ganglia. A greater understanding of the anatomy and histology of the human basal ganglia would also lead to major improvements in computational models of DBS, as most of the knowledge available about specific cell types and morphologies comes from non-human primates. Future DBS systems will likely allow for even more specific targeting through the implementation of more segmented leads, which can be used in a wide variety of combinations to activate very small populations of cells. As these systems and possibilities increase in complexity, computational models will also need to follow suit in order to provide the best symptom-specific targeting options for patients. Overall, an increased understanding of the variability present in the population of individuals with Parkinson's disease is an important step in improving outcomes for all patients.

REFERENCES

Abosch, A., Yacoub, E., Ugurbil, K., & Harel, N. (2010). An assessment of current brain targets for deep brain stimulation surgery with susceptibility-weighted imaging at 7 tesla. *Neurosurgery*, *67*(6), 1745–1756. https://doi.org/10.1227/NEU.0b013e3181f74105

Agnesi, F., Johnson, M. D., & Vitek, J. L. (2013). Deep brain stimulation: How does it work? *Handbook of Clinical Neurology*, *116*, 39–54. https://doi.org/10.1016/B978-0-444-53497-2.00004-8

Akram, H., Georgiev, D., Mahlknecht, P., Hyam, J., Foltynie, T., Limousin, P., … De Vita, E. (2017). Subthalamic deep brain stimulation sweet spots and hyperdirect cortical connectivity in Parkinson's disease. *NeuroImage*, *158*(July), 332–345. https://doi.org/10.1016/j.neuroimage.2017.07.012

Anderson, V. C., Burchiel, K. J., Hogarth, P., Favre, J., & Hammerstad, J. P. (2005). Pallidal vs subthalamic nucleus deep brain stimulation in Parkinson disease. *Archives of Neurology*, *62*(4), 554–560. https://doi.org/10.1001/archneur.62.4.554

Andersson, J. L. R., Skare, S., & Ashburner, J. (2003). How to correct susceptibility distortions in spin-echo echo-planar images: Application to diffusion tensor imaging. *NeuroImage*, *20*(2), 870–888. https://doi.org/10.1016/S1053-8119(03)00336-7

Angel, A., & Lemon, R. N. (1975). Sensorimotor cortical representation in the rat and the role of the cortex in the production of sensory myoclonic jerks. *The Journal of Physiology*, *248*(2), 465–488. https://doi.org/10.1113/jphysiol.1975.sp010984

Avecillas-Chasin, J. M., & Honey, C. R. (2020). Modulation of nigrofugal and pallidofugal pathways in deep brain stimulation for parkinson disease. *Neurosurgery*, *86*(4), E387–E397. https://doi.org/10.1093/neuros/nyz544

Baron, M. S., Sidib, M., Delong, M. R., & Smith, Y. (2001). Course of motor and associative pallidothalamic projections in monkeys. *Journal of Comparative Neurology*, *429*(3), 490–501. https://doi.org/10.1002/1096-9861(20010115)429:3<490::AID-CNE9>3.0.CO;2-K

Bartolic, A., Pirtosek, Z., Rozman, J., & Ribaric, S. (2005). Postural stability of Parkinson's disease patients is improved by decreasing rigidity. *European Journal of Neurology*, (12), 156–159.

Bates, D., Mächler, M., Bolker, B. M., & Walker, S. C. (2015). Fitting linear mixed-effects models using lme4. *Journal of Statistical Software*, *67*(1). https://doi.org/10.18637/jss.v067.i01

Behrens, T. E. J., Berg, H. J., Jbabdi, S., Rushworth, M. F. S., & Woolrich, M. W. (2007). Probabilistic diffusion tractography with multiple fibre orientations: What can we gain? *NeuroImage*, *34*(1), 144–155. https://doi.org/10.1016/j.neuroimage.2006.09.018

Berardelli, A., Sabra, A. F., & Hallett, M. (1983). Physiological mechanisms of rigidity in Parkinson's disease. *Journal of Neurology, Neurosurgery & Psychiatry*, *46*(1), 45–53. https://doi.org/10.1136/jnnp.46.1.45

Berry, R. B., Brooks, R., Gamaldo, C. E., Harding, S. M., & Lloyd, R. M. (2018). *AASM Manual for the Scoring of Sleep and Associated Events: Rules, Terminology, and Technical Specifications, Version 2.5*. American Academy of Sleep Medicine.

Bliwise, D. L., Trotti, L. M., Greer, S. A., Juncos, J. J., & Rye, D. B. (2010). Phasic muscle activity in sleep and clinical features of Parkinson disease. *Annals of Neurology*, *68*(3), 353–359. https://doi.org/10.1002/ana.22076

Boeve, B. F., Silber, M. H., Saper, C. B., Ferman, T. J., Dickson, D. W., Parisi, J. E., … Braak, H. (2007). Pathophysiology of REM sleep behaviour disorder and relevance to neurodegenerative disease. *Brain*, *130*(11), 2770–2788. https://doi.org/10.1093/brain/awm056

Boeve, Bradley F., Molano, J. R., Ferman, T. J., Lin, S.-C., Bieniek, K., Tippmann-Peikert, M., … Silber, M. H. (2013). Validation of the Mayo Sleep Questionnaire to Screen for REM Sleep Behavior Disorder in a Community-Based Sample. *Journal of Clinical Sleep Medicine, 09*(05), 475–480. https://doi.org/10.5664/jcsm.2670

Braak, H., Bohl, J. R., Müller, C. M., Rüb, U., de Vos, R. A. I., & Del Tredici, K. (2006). Stanley Fahn Lecture 2005: The staging procedure for the inclusion body pathology

associated with sporadic Parkinson's disease reconsidered. *Movement Disorders*, *21*(12), 2042–2051. https://doi.org/10.1002/mds.21065

Braak, H., Del Tredici, K., Rüb, U., De Vos, R. A. I., Jansen Steur, E. N. H., & Braak, E. (2003). Staging of brain pathology related to sporadic Parkinson's disease. *Neurobiology of Aging*, *24*(2), 197–211. https://doi.org/10.1016/S0197-4580(02)00065-9

Carpenter, M. B. (1991). *Core text of neuroanatomy. Fourth Edition.* (Vol. Williams &).

Carson, R. G., Riek, S., Mackey, D. C., Meichenbaum, D. P., Willms, K., Forner, M., & Byblow, W. D. (2004). Excitability changes in human forearm corticospinal projections and spinal reflex pathways during rhythmic voluntary movement of the opposite limb. *The Journal of Physiology*, *560*(3), 929–940. https://doi.org/10.1113/jphysiol.2004.069088

Chahine, L. M., Kauta, S. R., Daley, J. T., Cantor, C. R., & Dahodwala, N. (2014). Surface EMG activity during REM sleep in Parkinson's disease correlates with disease severity. *Parkinsonism & Related Disorders*, *20*(7), 766–771. https://doi.org/10.1016/j.parkreldis.2014.04.011

Chaturvedi, A., Butson, C. R., Lempka, S. F., Cooper, S. E., & McIntyre, C. C. (2010). Patient-specific models of deep brain stimulation: Influence of field model complexity on neural activation predictions. *Brain Stimulation*, *3*(2), 65–77. https://doi.org/10.1016/j.brs.2010.01.003

Chaturvedi, A., Luján, J. L., & McIntyre, C. C. (2013). Artificial neural network based characterization of the volume of tissue activated during deep brain stimulation. *Journal of Neural Engineering*, *10*(5). https://doi.org/10.1088/1741-2560/10/5/056023

Cheney, P. D., & Fetz, E. E. (1984). Corticomotoneuronal cells contribute to long-latency stretch reflexes in the rhesus monkey. *The Journal of Physiology*, *349*(1), 249–272. https://doi.org/10.1113/jphysiol.1984.sp015155

Delwaide, P. J. (2001). Parkinsonian rigidity. In *Functional Neurology* (Vol. 16, pp. 147–156).

Delwaide, P. J., Pepin, J.-L., De Pasqua, V., & Maertens de Noordhout, A. (2000). Projections from basal ganglia to tegmentum: a subcortical route for explaining the pathophysiology of Parkinson's disease signs? *Journal of Neurology*, *247*(S2), II75–II81. https://doi.org/10.1007/PL00007765

Delwaide, P. J., Pepin, J. L., & Maertens De Noordhout, A. (1991). Short-latency autogenic inhibition in patients with parkinsonian rigidity. *Annals of Neurology*, *30*(1), 83–89. https://doi.org/10.1002/ana.410300115

Dick, J. P. R., Rothwell, J. C., Day, B. L., Wise, R. J. S., Benecke, R., & Marsden, C. D. (1987). Modulation of the long-latency reflex to stretch by the supplementary motor area in humans. *Neuroscience Letters*, *75*(3), 349–354. https://doi.org/10.1016/0304-3940(87)90548-9

Duchin, Y., Abosch, A., Yacoub, E., Sapiro, G., & Harel, N. (2012). Feasibility of using ultra-high field (7 T) MRI for clinical surgical targeting. *PLoS ONE*, *7*(5). https://doi.org/10.1371/journal.pone.0037328

Duchin, Y., Shamir, R. R., Patriat, R., Kim, J., Vitek, J. L., Sapiro, G., & Harel, N. (2018). Patient-specific anatomical model for deep brain stimulation based on 7 Tesla MRI. *PLoS ONE*, *13*(8), 1–23. https://doi.org/10.1371/journal.pone.0201469

Fereshtehnejad, S. M., Yao, C., Pelletier, A., Montplaisir, J. Y., Gagnon, J. F., & Postuma, R. B. (2019). Evolution of prodromal Parkinson's disease and dementia with Lewy bodies: A prospective study. *Brain*, *142*(7), 2051–2067. https://doi.org/10.1093/brain/awz111

Ferreira-sánchez, M. D. R., Moreno-verdú, M., & Cano-de-la-cuerda, R. (2020). Quantitative measurement of rigidity in parkinson´s disease: A systematic review. *Sensors (Switzerland)*, *20*(3). https://doi.org/10.3390/s20030880

Fischl, B. (2012). FreeSurfer. *NeuroImage*, *62*(2), 774–781. https://doi.org/10.1016/j.neuroimage.2012.01.021

Folle, A. D., Paul, K. C., Bronstein, J. M., Keener, A. M., & Ritz, B. (2019). Clinical progression in Parkinson's disease with features of REM sleep behavior disorder: A population-based longitudinal study. *Parkinsonism & Related Disorders*, (July

2018), 1–7. https://doi.org/10.1016/j.parkreldis.2019.01.018

Follett, K. A., Weaver, F. M., Stern, M., Hur, K., Harris, C. L., Luo, P., … Reda, D. J. (2010). Pallidal versus Subthalamic Deep-Brain Stimulation for Parkinson's Disease. *New England Journal of Medicine*, *362*(22), 2077–2091. https://doi.org/10.1056/nejmoa0907083

Foltynie, T., Brayne, C., & Barker, R. A. (2002). The heterogeneity of idiopathic Parkinson's disease. *Journal of Neurology*, *249*(2), 138–145. https://doi.org/10.1007/PL00007856

Francois, J. G., Vingerhoets, Schulzer, M., Calne, D. B., & Snow, B. J. (1997). Which clinical sign of Parkinson's disease best reflects the nigrostriatal lesion? *Annals of Neurology*, *41*(1), 58–64. https://doi.org/10.1002/ana.410410111

Fung, V. S. C., Burne, J. A., & Morris, J. G. L. (2000). Objective quantification of resting and activated parkinsonian rigidity: A comparison of angular impulse and work scores. *Movement Disorders*, *15*(1), 48–55. https://doi.org/10.1002/1531-8257(200001)15:1<48::AID-MDS1009>3.0.CO;2-E

Gabriel, S., Lau, R. W., & Gabriel, C. (1996a). Physics in Medicine & Biology. The dielectric properties of biological tissues: III. Parametric models for the dielectric spectrum of tissues. *Phys. Med. Biol. Phys. Med. Biol*, *41*(41), 2251–2269. Retrieved from http://iopscience.iop.org/article/10.1088/0031-9155/41/11/002/pdf

Gabriel, S., Lau, R. W., & Gabriel, C. (1996b). The dielectric properties of biological tissues: II. Measurements in the frequency range 10 Hz to 20 GHz. *Physics in Medicine and Biology*, *41*(11), 2251–2269. https://doi.org/10.1088/0031-9155/41/11/002

Goetz, C. G., Tilley, B. C., Shaftman, S. R., Stebbins, G. T., Fahn, S., Martinez-Martin, P., … Zweig, R. M. (2008). Movement Disorder Society-Sponsored Revision of the Unified Parkinson's Disease Rating Scale (MDS-UPDRS): Scale presentation and clinimetric testing results. *Movement Disorders*, *23*(15), 2129–2170. https://doi.org/10.1002/mds.22340

Greenland, J. C., Williams-Gray, C. H., & Barker, R. A. (2019). The clinical

heterogeneity of Parkinson's disease and its therapeutic implications. *European Journal of Neuroscience*, *49*(3), 328–338. https://doi.org/10.1111/ejn.14094

Gunalan, K., Chaturvedi, A., Howell, B., Duchin, Y., Lempka, S. F., Patriat, R., … McIntyre, C. C. (2017). Creating and parameterizing patient-specific deep brain stimulation pathway-activation models using the hyperdirect pathway as an example. *PLoS ONE*, *12*(4), 1–19. https://doi.org/10.1371/journal.pone.0176132

Haba-Rubio, J., Frauscher, B., Marques-Vidal, P., Toriel, J., Tobback, N., Andries, D., … Heinzer, R. (2018). Prevalence and determinants of rapid eye movement sleep behavior disorder in the general population. *Sleep*, *41*(2), 1–8. https://doi.org/10.1093/sleep/zsx197

Hamada, M., Ugawa, Y., Tsuji, S., Kaji, R., Tobimatsu, S., Nakajima, K., … Tanaka, T. (2008). High-frequency rTMS over the supplementary motor area for treatment of Parkinson's disease. *Movement Disorders*, *23*(11), 1524–1531. https://doi.org/10.1002/mds.22168

Harris, P. A., Taylor, R., Thielke, R., Payne, J., Gonzalez, N., & Conde, J. G. (2009). Research electronic data capture (REDCap)-A metadata-driven methodology and workflow process for providing translational research informatics support. *Journal of Biomedical Informatics*, *42*(2), 377–381. https://doi.org/10.1016/j.jbi.2008.08.010

Hashimoto, T., Elder, C. M., Okun, M. S., Patrick, S. K., & Vitek, J. L. (2003). Stimulation of the subthalamic nucleus changes the firing pattern of pallidal neurons. *Journal of Neuroscience*, *23*(5), 1916–1923. https://doi.org/10.1523/jneurosci.23-05-01916.2003

Heckman, C. J., Gorassini, M. A., & Bennett, D. J. (2005). Persistent inward currents in motoneuron dendrites: Implications for motor output. *Muscle and Nerve*, *31*(2), 135–156. https://doi.org/10.1002/mus.20261

Heckman, C. J., Mottram, C., Quinlan, K., Theiss, R., & Schuster, J. (2009). Motoneuron excitability: The importance of neuromodulatory inputs. *Clinical Neurophysiology*, *120*(12), 2040–2054. https://doi.org/10.1016/j.clinph.2009.08.009

Hegeman, D. J., Hong, E. S., Hernández, V. M., & Chan, C. S. (2016). The external

globus pallidus: Progress and perspectives. *European Journal of Neuroscience*, *43*(10), 1239–1265. https://doi.org/10.1111/ejn.13196

Hines, M. L., & Carnevale, N. T. (1997). The NEURON Simulation Environment. *Neural Computation*, *9*(6), 1179–1209. https://doi.org/10.1162/neco.1997.9.6.1179

Hong, M., Perlmutter, J. S., & Earhart, G. M. (2007). Enhancement of rigidity in Parkinson's disease with activation. *Movement Disorders*, *22*(8), 1164–1168. https://doi.org/10.1002/mds.21524

Horn, A., Li, N., Dembek, T. A., Kappel, A., Boulay, C., Ewert, S., … Kühn, A. A. (2019). NeuroImage Lead-DBS v2 : Towards a comprehensive pipeline for deep brain stimulation imaging Region of Interest. *NeuroImage*, *184*(August 2018), 293–316. https://doi.org/10.1016/j.neuroimage.2018.08.068

Hortobágyi, T., Taylor, J. L., Petersen, N. T., Russell, G., & Gandevia, S. C. (2003). Changes in Segmental and Motor Cortical Output With Contralateral Muscle Contractions and Altered Sensory Inputs in Humans. *Journal of Neurophysiology*, *90*(4), 2451–2459. https://doi.org/10.1152/jn.01001.2002

Howell, B., & McIntyre, C. C. (2017). Role of Soft-Tissue Heterogeneity in Computational Models of Deep Brain Stimulation. *Brain Stimulation*, *10*(1), 46–50. https://doi.org/10.1016/j.brs.2016.09.001

Hummelsheim, H., Wiesendanger, M., & Bianchetti, M. (1986). The supplementary motor area modulates perturbations-evoked discharges of neurones in the precentral motor cortex. *Neuroscience Letters*, *67*, 119–122.

Innocenti, G. M., Vercelli, A., & Caminiti, R. (2014). The diameter of cortical axons depends both on the area of origin and target. *Cerebral Cortex*, *24*(8), 2178–2188. https://doi.org/10.1093/cercor/bht070

Jenkinson, M., Beckmann, C. F., Behrens, T. E. J., Woolrich, M. W., & Smith, S. M. (2012). Fsl. *NeuroImage*, *62*(2), 782–790. https://doi.org/10.1016/j.neuroimage.2011.09.015

Jenkinson, M., & Smith, S. (2001). A global optimisation method for robust affine registration of brain images. *Medical Image Analysis*, *5*(2), 143–156.

https://doi.org/10.1016/S1361-8415(01)00036-6

Johnson, M. D., & McIntyre, C. C. (2008). Quantifying the neural elements activated and inhibited by globus pallidus deep brain stimulation. *Journal of Neurophysiology*, *100*(5), 2549–2563. https://doi.org/10.1152/jn.90372.2008

Johnson, M. D., Miocinovic, S., McIntyre, C. C., & Vitek, J. L. (2008). Mechanisms and Targets of Deep Brain Stimulation in Movement Disorders. *Neurotherapeutics*, *5*(2), 294–308. https://doi.org/10.1016/j.nurt.2008.01.010

Johnson, M. D., Zhang, J., Ghosh, D., McIntyre, C. C., & Vitek, J. L. (2012). Neural targets for relieving parkinsonian rigidity and bradykinesia with pallidal deep brain stimulation. *Journal of Neurophysiology*, *108*(2), 567–577. https://doi.org/10.1152/jn.00039.2012

Johnson, M. T. V., Mendez, A., Kipnis, A. N., Silverstein, P., Zwiebel, F., & Ebner, T. J. (1994). Acute effects of levodopa on wrist movement in parkinson's disease: Kinematics, volitional EMG modulation and reflex amplitude modulation. *Brain*, *117*(6), 1409–1422. https://doi.org/10.1093/brain/117.6.1409

Kalia, L. V., & Lang, A. E. (2015). Parkinson's disease. *The Lancet*, *386*(9996), 896–912. https://doi.org/10.1016/S0140-6736(14)61393-3

Karlawish, J., Cary, M., Moelter, S. T., Siderowf, A., Sullo, E., Xie, S., & Weintraub, D. (2013). Cognitive impairment and PD patients' capacity to consent to research. *Neurology*, *81*(9), 801–807. https://doi.org/10.1212/WNL.0b013e3182a05ba5

Knopman, D. S. (2014). NINDS PD2014 : Final Research Recommendations, (10), 1–21.

Kowal, S. L., Dall, T. M., Chakrabarti, R., Storm, M. V., & Jain, A. (2013). The current and projected economic burden of Parkinson's disease in the United States. *Movement Disorders*, *28*(3), 311–318. https://doi.org/10.1002/mds.25292

Krack, P., Pollak, P., Limousin, P., Hoffmann, D., Benazzouz, A., Le Bas, J. F., … Benabid, A. L. (1998). Opposite motor effects of pallidal stimulation in Parkinson's disease. *Annals of Neurology*, *43*(2), 180–192. https://doi.org/10.1002/ana.410430208

Krack, Paul, Fraix, V., Mendes, A., Benabid, A. L., & Pollak, P. (2002). Postoperative management of subthalamic nucleus stimulation for parkinson's disease. *Movement Disorders*, *17*(SUPPL. 3), 188–197. https://doi.org/10.1002/mds.10163

Kumru, H., Santamaria, J., Tolosa, E., & Iranzo, A. (2007). Relation between subtype of Parkinson's disease and REM sleep behavior disorder. *Sleep Medicine*, *8*(7–8), 779–783. https://doi.org/10.1016/j.sleep.2007.02.005

Lenglet, C., Abosch, A., Yacoub, E., de Martino, F., Sapiro, G., & Harel, N. (2012). Comprehensive in vivo mapping of the human basal ganglia and thalamic connectome in individuals using 7T MRI. *PLoS ONE*, *7*(1). https://doi.org/10.1371/journal.pone.0029153

Lenz, F. A., Tatton, W. G., & Tasker, R. R. (1983). The effect of cortical lesions on the electromyographic response to joint displacement in the squirrel monkey forelimb. *J Neurosci*, *3*(4), 795–805. Retrieved from https://www.ncbi.nlm.nih.gov/pubmed/6834106

Lenz, F., Tatton, W., & Tasker, R. (1983). Electromyographic response to displacement of different forelimb joints in the squirrel monkey. *The Journal of Neuroscience*, *3*(4), 783–794. https://doi.org/10.1523/JNEUROSCI.03-04-00783.1983

Lewis, S. J. G., Foltynie, T., Blackwell, A. D., Bobbins, T. W., Owen, A. M., & Barker, R. A. (2005). Heterogeneity of Parkinson's disease in the early clinical stages using a data driven approach. *Journal of Neurology, Neurosurgery and Psychiatry*, *76*(3), 343–348. https://doi.org/10.1136/jnnp.2003.033530

Liewald, D., Miller, R., Logothetis, N., Wagner, H. J., & Schüz, A. (2014). Distribution of axon diameters in cortical white matter: an electron-microscopic study on three human brains and a macaque. *Biological Cybernetics*, *108*(5), 541–557. https://doi.org/10.1007/s00422-014-0626-2

Linn-Evans, M. E., Petrucci, M. N., Amundsen Huffmaster, S. L., Chung, J. W., Tuite, P. J., Howell, M. J., … MacKinnon, C. D. (2020). REM sleep without atonia is associated with increased rigidity in patients with mild to moderate Parkinson's disease. *Clinical Neurophysiology*, *131*(8), 2008–2016.

https://doi.org/10.1016/j.clinph.2020.04.017

MacKinnon, C D. (2018). Sensorimotor anatomy of gait, balance, and falls. *Handb Clin Neurol*, *159*, 3–26. https://doi.org/10.1016/B978-0-444-63916-5.00001-X

MacKinnon, Colum D., Verrier, M. C., & Tatton, W. G. (2000). Motor cortical potentials precede long-latency EMG activity evoked by imposed displacements of the human wrist. *Experimental Brain Research*, *131*(4), 477–490. https://doi.org/10.1007/s002219900317

Marinus, J., & van Hilten, J. J. (2015). The significance of motor (A)symmetry in Parkinson's disease. *Movement Disorders*, *30*(3), 379–385. https://doi.org/10.1002/mds.26107

Marras, C., Beck, J. C., Bower, J. H., Roberts, E., Ritz, B., Ross, G. W., … Tanner, C. (2018). Prevalence of Parkinson's disease across North America. *Parkinson's Disease*, *4*(1), 1–7. https://doi.org/10.1038/s41531-018-0058-0

Martin, W. E., Loewenson, R. B., Resch, J. A., & Baker, A. B. (1973). Parkinson's disease: Clinical analysis of 100 patients. *Neurology*, *23*(8), 783–783. https://doi.org/10.1212/WNL.23.8.783

Martinez-Gonzalez, C., Bolam, J. P., & Mena-Segovia, J. (2011). Topographical organization of the pedunculopontine nucleus. *Front Neuroanat*, *5*, 22. https://doi.org/10.3389/fnana.2011.00022

Mathai, A., Wichmann, T., & Smith, Y. (2013). More than meets the eye-myelinated axons crowd the subthalamic nucleus. *Movement Disorders*, *28*(13), 1811–1815. https://doi.org/10.1002/mds.25603

Matias, C. M., Mehanna, R., Cooper, S. E., Amit, A., Lempka, S. F., Silva, D., … MacHado, A. G. (2015). Correlation among anatomic landmarks, location of subthalamic deep brain stimulation electrodes, stimulation parameters, and side effects during programming monopolar review. *Operative Neurosurgery*, *11*(1), 99–108. https://doi.org/10.1227/NEU.0000000000000645

Matthews, P. B. C. C. (1991). The human stretch reflex and the motor cortex. *Trends in Neurosciences*, *14*(3), 87–91. https://doi.org/10.1016/0166-2236(91)90064-2

McIntyre, C. C., Grill, W. M., Sherman, D. L., & Thakor, N. V. (2004). Cellular Effects of Deep Brain Stimulation: Model-Based Analysis of Activation and Inhibition. *Journal of Neurophysiology*, *91*(4), 1457–1469. https://doi.org/10.1152/jn.00989.2003

McIntyre, C. C., Richardson, A. G., & Grill, W. M. (2002). Modeling the excitability of mammalian nerve fibers: Influence of afterpotentials on the recovery cycle. *Journal of Neurophysiology*, *87*(2), 995–1006. https://doi.org/10.1152/jn.00353.2001

Mollenhauer, B., Trautmann, E., Sixel-Döring, F., Wicke, T., Ebentheuer, J., Schaumburg, M., … Trenkwalder, C. (2013). Nonmotor and diagnostic findings in subjects with de novo Parkinson disease of the DeNoPa cohort. *Neurology*, *81*(14), 1226–1234.

Mortimer, J. A., & Webster, D. D. (1979). Evidence for a quantitative association between EMG stretch responses and Parkinsonian rigidity. *Brain Research*, *162*(1), 169–173. https://doi.org/10.1016/0006-8993(79)90768-6

Mutch, W. J., Strudwick, A., Roy, S. K., & Downie, A. W. (1986). Parkinson's disease: disability, review, and management. *British Medical Journal*, *293*(September), 611–629. https://doi.org/10.1017/CHO9780511974007.028

Noecker, A., Gilber-Frankemolle, A., Howell, B., Petersen, M., Balta Beylergil, S., Shakh, A., & McIntyre, C. (2020). StimVision v2: Examples and Applications in Subthalamic Deep Brain Stimulation for Parkinson's Disease. *Neuromodulation: Technology at the Neural Interface*, *24*(2), 248–258.

Noecker, A. M., Choi, K. S., Riva-Posse, P., Gross, R. E., Mayberg, H. S., & McIntyre, C. C. (2018). StimVision Software: Examples and Applications in Subcallosal Cingulate Deep Brain Stimulation for Depression. *Neuromodulation: Technology at the Neural Interface*, *21*(2), 191–196. https://doi.org/10.1111/ner.12625

Odekerken, V. J. J., van Laar, T., Staal, M. J., Mosch, A., Hoffmann, C. F. E., Nijssen, P. C. G., … de Bie, R. M. A. (2013). Subthalamic nucleus versus globus pallidus bilateral deep brain stimulation for advanced Parkinson's disease (NSTAPS study): A randomised controlled trial. *The Lancet Neurology*, *12*(1), 37–44.

https://doi.org/10.1016/S1474-4422(12)70264-8

Parent, A., Sato, F., Wu, Y., Gauthier, J., Lévesque, M., & Parent, M. (2000). Organization of the basal ganglia: The importance of axonal collateralization. *Trends in Neurosciences*, *23*(10 SUPPL.), 20–27. https://doi.org/10.1016/S1471-1931(00)00022-7

Parent, M., & Parent, A. (2004). The pallidofugal motor fiber system in primates. *Parkinsonism and Related Disorders*, *10*(4), 203–211. https://doi.org/10.1016/j.parkreldis.2004.02.007

Patriat, R., Cooper, S. E., Duchin, Y., Niederer, J., Lenglet, C., Aman, J., … Harel, N. (2018). Individualized tractography-based parcellation of the globus pallidus pars interna using 7T MRI in movement disorder patients prior to DBS surgery. *NeuroImage*, *178*(February 2018), 198–209. https://doi.org/10.1016/j.neuroimage.2018.05.048

Patrick, S. K., Denington, A. A., Gauthier, M. J. A., Gillard, D. M., & Prochazka, A. (2001). Quantification of the UPDRS rigidity scale. *IEEE Transactions on Neural Systems and Rehabilitation Engineering*, *9*(1), 31–41. https://doi.org/10.1109/7333.918274

Perera, T., Lee, W.-L., Jones, M., Tan, J. L., Proud, E. L., Begg, A., … McDermott, H. J. (2019). A palm-worn device to quantify rigidity in Parkinson's disease. *Journal of Neuroscience Methods*, *317*, 113–120. https://doi.org/10.1016/j.jneumeth.2019.02.006

Petersen, M. V., Mlakar, J., Haber, S. N., Parent, M., Smith, Y., Strick, P. L., … McIntyre, C. C. (2019). Holographic Reconstruction of Axonal Pathways in the Human Brain. *Neuron*, *104*(6), 1056-1064.e3. https://doi.org/10.1016/j.neuron.2019.09.030

Postuma, R. B., Gagnon, J. F., Vendette, M., Charland, K., & Montplaisir, J. (2008). REM sleep behaviour disorder in Parkinson's disease is associated with specific motor features. *Journal of Neurology, Neurosurgery & Psychiatry*, *79*(10), 1117–1121. https://doi.org/10.1136/jnnp.2008.149195

Postuma, R. B., Lang, A. E., Gagnon, J. F., Pelletier, A., & Montplaisir, J. Y. (2012). How does parkinsonism start? Prodromal parkinsonism motor changes in idiopathic REM sleep behaviour disorder. *Brain*, *135*(6), 1860–1870. https://doi.org/10.1093/brain/aws093

Postuma, Ronald B., Berg, D., Stern, M., Poewe, W., Olanow, C. W., Oertel, W., … Deuschl, G. (2015). MDS clinical diagnostic criteria for Parkinson's disease. *Movement Disorders*, *30*(12), 1591–1601. https://doi.org/10.1002/mds.26424

Postuma, Ronald B., Iranzo, A., Hu, M., Högl, B., Boeve, B. F., Manni, R., … Pelletier, A. (2019). Risk and predictors of dementia and parkinsonism in idiopathic REM sleep behaviour disorder: a multicentre study. *Brain*, *142*(3), 744–759. https://doi.org/10.1093/brain/awz030

Powell, D., Hanson, N., Joseph Threlkeld, A., Fang, X., & Xia, R. (2011). Enhancement of parkinsonian rigidity with contralateral hand activation. *Clinical Neurophysiology*, *122*(8), 1595–1601. https://doi.org/10.1016/j.clinph.2011.01.010

Prochazka, A., Bennett, D. J., Stephens, M. J., Patrick, S. K., Sears-Duru, R., Roberts, T., & Jhamandas, J. H. (1997). Measurement of rigidity in Parkinson's disease. *Movement Disorders*, *12*(1), 24–32. https://doi.org/10.1002/mds.870120106

R Core Team. (2021). R: A language and environment for statistical computing. *R Foundation for Statistical Computing*. Retrieved from https://www.r-project.org

Romenets, S. R., Gagnon, J.-F., Latreille, V., Panniset, M., Chouinard, S., Montplaisir, J., & Postuma, R. B. (2012). Rapid eye movement sleep behavior disorder and subtypes of Parkinson's disease. *Movement Disorders*, *27*(8), 996–1003. https://doi.org/10.1002/mds.25086

Rothwell, J. C., Obeso, J. A., Traub, M. M., & Marsden, C. D. (1983). The behaviour of the long-latency stretch reflex in patients with Parkinson's disease. *Journal of Neurology, Neurosurgery & Psychiatry*, *46*(1), 35–44. https://doi.org/10.1136/jnnp.46.1.35

Sabatini, U., Boulanouar, K., Fabre, N., Chollet, F., Berry, I., Colonnese, C., … Rascol, O. (2000). Cortical motor reorganization in akinetic Parkinsonian patients: A

functional magnetic resonance imaging study. *Brain*, *7*(4 PART II), 394–403. https://doi.org/10.1016/s1053-8119(18)31309-0

Sato, F., Lavallée, P., Lévesque, M., & Parent, A. (2000). Single-axon tracing study of neurons of the external segment of the globus pallidus in primate. *Journal of Comparative Neurology*, *417*(1), 17–31. https://doi.org/10.1002/(SICI)1096-9861(20000131)417:1<17::AID-CNE2>3.0.CO;2-I

Schenck, C. H., Boeve, B. F., & Mahowald, M. W. (2013). Delayed emergence of a parkinsonian disorder or dementia in 81% of older men initially diagnosed with idiopathic rapid eye movement sleep behavior disorder: a 16-year update on a previously reported series. *Sleep Medicine*, *14*(8), 744–748. https://doi.org/10.1016/j.sleep.2012.10.009

Schmidt, C., & Van Rienen, U. (2012). Modeling the field distribution in deep brain stimulation: The influence of anisotropy of brain tissue. *IEEE Transactions on Biomedical Engineering*, *59*(6), 1583–1592. https://doi.org/10.1109/TBME.2012.2189885

Smith, S. M. (2002). Fast robust automated brain extraction. *Human Brain Mapping*, *17*(3), 143–155. https://doi.org/10.1002/hbm.10062

Starr, P. A. (2002). Placement of deep brain stimulators into the subthalamic nucleus or globus pallidus internus: Technical approach. *Stereotactic and Functional Neurosurgery*, *79*(3–4), 118–145. https://doi.org/10.1159/000070828

Starr, P. A., Vitek, J. L., DeLong, M., & Bakay, R. A. E. (1999). Magnetic resonance imaging-based stereotactic localization of the globus pallidus and subthalamic nucleus. *Neurosurgery*, *44*(2), 303–314. https://doi.org/10.1097/00006123-199902000-00031

Tatton, W. G. G., & Lee, R. G. G. (1975). Evidence for abnormal long-loop reflexes in rigid Parkinsonian patients. *Brain Research*, *100*(3), 671–676. https://doi.org/10.1016/0006-8993(75)90167-5

Tomlinson, C. L., Stowe, R., Patel, S., Rick, C., Gray, R., & Clarke, C. E. (2010). Systematic review of levodopa dose equivalency reporting in Parkinson’s disease.

Movement Disorders, *25*(15), 2649–2653. https://doi.org/10.1002/mds.23429

Travis, A. M. (1955). Neurological deficiencies following supplementary motor area lesions in Macaca mulatta. *Brain*, *78*(2), 174–175. https://doi.org/10.1093/brain/78.2.174

Vitek, J. L., Hashimoto, T., Peoples, J., DeLong, M. R., & Bakay, R. A. E. (2004). Acute stimulation in the external segment of the globus pallidus improves parkinsonian motor signs. *Movement Disorders*, *19*(8), 907–915. https://doi.org/10.1002/mds.20137

Vitek, J. L., Zhang, J., Hashimoto, T., Russo, G. S., & Baker, K. B. (2012). External pallidal stimulation improves parkinsonian motor signs and modulates neuronal activity throughout the basal ganglia thalamic network. *Experimental Neurology*, *233*(1), 581–586. https://doi.org/10.1016/j.expneurol.2011.09.031

Vu, T. C., Nutt, J. G., & Holford, N. H. G. (2012). Progression of motor and nonmotor features of Parkinson's disease and their response to treatment. *British Journal of Clinical Pharmacology*, *74*(2), 267–283. https://doi.org/10.1111/j.1365-2125.2012.04192.x

Weaver, F. M., Follett, K. A., Hur, K., Ippolito, D., & Stern, M. B. (2005). Deep brain stimulation in Parkinson disease: a metaanalysis of patient outcomes. *Journal of Neurosurgery*, *103*, 956–967.

Weaver, F. M., Follett, K. A., Stern, M., Luo, P., Harris, C. L., Hur, K., … Reda, D. J. (2012). Randomized trial of deep brain stimulation for Parkinson disease: Thirty-six-month outcomes. *Neurology*, *79*(1), 55–65. https://doi.org/10.1212/WNL.0b013e31825dcdc1

Williams, N. R., Foote, K. D., & Okun, M. S. (2014). Subthalamic Nucleus Versus Globus Pallidus Internus Deep Brain Stimulation: Translating the Rematch Into Clinical Practice. *Movement Disorders Clinical Practice*, *1*(1), 24–35. https://doi.org/10.1002/mdc3.12004

Winogrodzka, A., Wagenaar, R. C., Booij, J., & Wolters, E. C. (2005). Rigidity and bradykinesia reduce interlimb coordination in Parkinsonian gait. *Archives of*

Physical Medicine and Rehabilitation, *86*(2), 183–189. https://doi.org/10.1016/j.apmr.2004.09.010

Woolrich, M. W., Jbabdi, S., Patenaude, B., Chappell, M., Makni, S., Behrens, T., … Smith, S. M. (2009). Bayesian analysis of neuroimaging data in FSL. *NeuroImage*, *45*(1 Suppl), S173–S186. https://doi.org/10.1016/j.neuroimage.2008.10.055

Xia, R, Markopoulou, K., Puumala, S. E., & Rymer, W. Z. (2006). A comparison of the effects of imposed extension and flexion movements on Parkinsonian rigidity. *Clin Neurophysiol*, *117*(10), 2302–2307. https://doi.org/10.1016/j.clinph.2006.06.176

Xia, Ruiping. (2011). Physiological and Biomechanical Analyses of Rigidity in Parkinson's Disease. In A. Qayyum Rana (Ed.), *Etiology and Pathophysiology of Parkinson's Disease* (p. 13). IntechOpen. https://doi.org/https://doi.org/10.5772/17849

Xia, Ruiping, & Rymer, W. Z. (2004). The role of shortening reaction in mediating rigidity in Parkinson's disease. *Experimental Brain Research*, *156*(4), 524–528. https://doi.org/10.1007/s00221-004-1919-9

Xia, Ruiping, Sun, J., & Threlkeld, A. J. (2009). Analysis of interactive effect of stretch reflex and shortening reaction on rigidity in Parkinson's disease. *Clinical Neurophysiology*, *120*(7), 1400–1407. https://doi.org/10.1016/j.clinph.2009.05.001

Xu, W., Miocinovic, S., Zhang, J., Baker, K. B., McIntyre, C. C., & Vitek, J. L. (2011). Dissociation of motor symptoms during deep brain stimulation of the subthalamic nucleus in the region of the internal capsule. *Experimental Neurology*, *228*(2), 294–297. https://doi.org/10.1016/j.expneurol.2010.08.007

Yahr, M. D., Duvoisin, R. C., Schear, M. J., Barrett, R. E., & Hoehn, M. M. (1969). Treatment of parkinsonism with levodopa. *Archives of Neurology*, *21*(4), 343–354. https://doi.org/10.1001/archneur.1969.00480160015001

Yelnik, J., Damier, P., Bejjani, B. P., Francois, C., Gervais, D., Dormont, D., … Agid, Y. (2000). Functional mapping of the human globus pallidus: Contrasting effect of stimulation in the internal and external pallidum in Parkinson's disease. *Neuroscience*, *101*(1), 77–87. https://doi.org/10.1016/S0306-4522(00)00364-X

Yousif, N., Bayford, R., & Liu, X. (2008). The influence of reactivity of the electrode-brain interface on the crossing electric current in therapeutic deep brain stimulation. *Neuroscience*, *156*(3), 597–606. https://doi.org/10.1016/j.neuroscience.2008.07.051

Zhang, Jia, Xu, C.-Y., & Liu, J. (2017). Meta-analysis on the prevalence of REM sleep behavior disorder symptoms in Parkinson's disease. *BMC Neurology*, *17*(1), 23. https://doi.org/10.1186/s12883-017-0795-4

Zhang, Jianyu, Wang, Z. I., Baker, K. B., & Vitek, J. L. (2012). Effect of globus pallidus internus stimulation on neuronal activity in the pedunculopontine tegmental nucleus in the primate model of Parkinson's disease. *Experimental Neurology*, *233*(1), 575–580. https://doi.org/10.1016/j.expneurol.2011.07.007

Zhang, Y., Brady, M., & Smith, S. (2001). Segmentation of brain MR images through a hidden Markov random field model and the expectation-maximization algorithm. *IEEE Transactions on Medical Imaging*, *20*(1), 45–57. https://doi.org/10.1109/42.906424